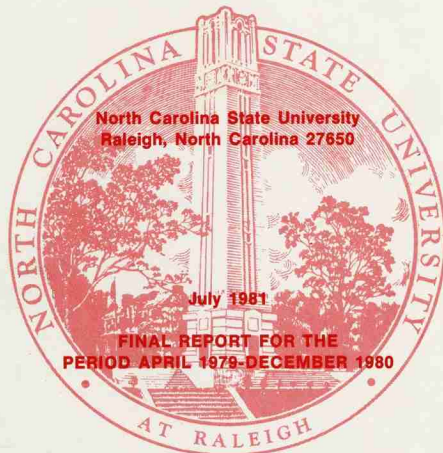


YEAR-ROUND SOLAR-ENERGY UTILIZATION IN BULK-CURING/GREENHOUSE SYSTEM

B. K. HUANG

Professor

**Biological and Agricultural
Engineering Department**



Prepared for
**UNITED STATES DEPARTMENT OF ENERGY
UNITED STATES DEPARTMENT OF AGRICULTURE**
Washington, D. C.



YEAR-ROUND SOLAR-ENERGY UTILIZATION

IN

BULK-CURING/GREENHOUSE SYSTEM

B.K. HUANG

Professor of Biological and Agricultural Engineering

Research Performed Under Grant No. 12-14-7001-818

July 1981

North Carolina State University
Biological and Agricultural Engineering Department
Raleigh, North Carolina 27650

PREFACE

This research project "Year-Round Solar-Energy Utilization in Bulk-Curing/Greenhouse System" was conducted at the North Carolina State University, Biological and Agricultural Engineering Department, Raleigh, N.C. 27650. It was initiated under the National Science Foundation Grant Number PTP74-17622 in 1974, and later transferred to the Energy Research and Development Administration. Then the program was reviewed quarterly and continuously supported by the U.S. Department of Agriculture and Department of Energy until the end of 1980.

The author wishes to acknowledge the partial sponsorship for the research by the National Science Foundation, the Energy Research and Development Administration, the U.S. Department of Agriculture, the Department of Energy, the North Carolina Energy Institute, the North Carolina Tobacco Foundation, and the North Carolina Agricultural Research Service. He wish to express his appreciation to: Harrington Manufacturing Company, Powell Manufacturing Company and Taylor Manufacturing Company for assistance in providing necessary equipment; Dr. M.N. Ozisik, Professor, Dr. M. Toksoy, Visiting Assistant Professor, and Ms. N.M. El-Shaik, Graduate Assistant, of Mechanical and Aerospace Engineering, Mr. C.G. Bowers, Jr., Instructor, and Mr. A.H. Nassar, Graduate Assistant, of Biological and Agricultural Engineering, P. Oppenheim, Engineering Extension Specialist, Mr. W.R. Baker, Superintendent, and Mr. A.T. Wood, Tobacco Supervisor, of Central Crops Research Station for consultation and participating in field tests; Mrs. Brenda Mason, Secretary of Biological and Agricultural Engineering for her typing of the manuscript; and

ABSTRACT

The greenhouse solar system (bulk-curing/greenhouse system or solar barn) is a large solar collector in which the curing and drying process or plant production process is taking place for effective year-round solar energy utilization in agricultural production. The structure and equipment constitute a solar collector to allow competitive initial cost for the solar unit as compared to that for a conventional drying unit. The previous seven-year study on this multiple-purpose system has indicated that an effective solar energy utilization can be achieved for on-farm tobacco and peanut curing and greenhouse plant production.

Full scale tobacco cures with the solar system have demonstrated quality tobacco curing with a 47 to 54 percent fuel savings for this system as compared to a conventional bulk curing barn. The microcomputer control of tobacco bulk curing process was first implemented and successfully applied to maximize solar energy utilization as well as automated data acquisition and control. The rotary solar drum unit was designed to dry peanuts and other agricultural crops in drying mode operation applying the principle of reversible-flow, periodic agitation, and low-temperature solar drying resulting in significant fuel savings. The unit is convertible to a rotary layer automated seedling production system to be used in greenhouse mode operation.

At the end of the curing and drying season the solar barn has been converted into a solar greenhouse to demonstrate the automated production of flowers, cucumbers, tomatoes, various seedlings and tobacco transplants. During greenhouse mode of operation, both full scale hydroponic tomato production and automated tobacco transplant production were studied in the solar barn. Germination rates of 95-97 percent and uniform growth in the early

stages of transplant growth have been achieved in seedling production. Growth and yield studies have shown that solar barn grown seedlings adapted to fully automatic transplanting and that better growth and yield can be achieved from these seedlings. A microcomputer based system was designed to monitor and control the greenhouse environmental conditions using hardware control devices and software programming to achieve desired system performance.

System design concept, theoretical considerations, mathematical models and analyses have been developed for solar drying mode operation. The simulation results conformed favorably to the measured data. Analogous circuit simulation models of a greenhouse solar drying system has been developed to study the system performance and key variable interactions with digital simulation techniques. Results show that the computer predictions are in good agreement with the measured thermal behavior of the solar drier.

The basic concept of solar barn has been adapted to conventional bulk curing box barns. The on-farm full scale tests have also shown that significant fuel savings have been achieved in solar bulk curing of tobacco in large containers. Efforts are under way for design and construction of a latent heat storage system to be used as an integrated part of the greenhouse solar system to replace the sensible heat rock bed storage system.

The greenhouse solar system provides an efficient means of utilizing solar energy all the year round for agricultural production. In this multipurpose farm structure, attention to costs of construction and materials resulted in the greenhouse bulk curing solar barn system costing slightly less than that of conventional bulk barn of equivalent capacity.

TABLE OF CONTENTS

	Page
PREFACE	ii
ABSTRACT	iv
LIST OF FIGURES	vii
LIST OF TABLES	x
INTRODUCTION	1
ENERGY FOR TOBACCO CURING	5
SYSTEM DESIGN AND DESCRIPTION	11
THEORETICAL CONSIDERATIONS AND ANALYSIS	17
Direct Solar Radiation	17
Diffuse Solar Radiation	20
Total Radiation Incident Upon the Plane Surfaces	
Toward South and North	20
Total Solar Radiation	22
System Efficiency	23
Solar Heating of the Air	25
Heat and Mass Transfer of Drying	31
Dynamic System Analysis	35
MICROCOMPUTER DATA ACQUISITION AND CONTROL SYSTEM	36
FIELD TEST RESULTS AND DISCUSSION	39
Curing and Drying Mode Operations	39
Greenhouse Mode Operations	60
CIRCUIT SIMULATION ANALYSIS AND VERIFICATION	68
Thermal Circuit Representing Greenhouse	
Solar Drying System	76
Simulation Results and Discussion	79
LATENT HEAT STORAGE SYSTEM DESIGN AND CONSTRUCTION	83
Latent Heat Storage System	86
Experimental Setup	93
Methods and Procedures	98
REFERENCES	99

LIST OF FIGURES

Figure		Page
1.	Greenhouse Solar System Setup: (a) Tobacco Curing Mode; (b) Peanut Curing or Grain Drying Mode; (c) Illustration of Typical Air Flow Patterns for Solar Drying and Furnace Drying.	12
2.	Greenhouse Solar System Setup for Greenhouse Mode Showing Typical Air Flow Pattern: (a) Stationary and Rotary Layer Automated Seedling Production Systems Utilizing Portable Frames and Rotary Drums; (b) Hydroponic Plant Production with Liquid Solar Heat Collection and Storage System.	15
3.	Schematic of Greenhouse Solar Bulk Curing and Drying System.	16
4.	Direct Solar Radiation Incident upon a Semicylindrical Receiver.	16
5.	Incident Diffuse Radiation Scattered by Sky and Reflected by Ground on a Semicylindrical Receiver.	21
6.	Incident Solar Radiation on a Semicylindrical Receiver.	21
7.	Functional Description of Microcomputer Based Control System.	37
8.	Field Operation of Greenhouse Solar System: (a) Tobacco Curing Mode; (b) Peanut Curing or Grain Drying Mode.	40
9.	Yellowing and First Day Leaf Drying.	41
10.	Leaf and Stem Drying.	42
11.	System Performance of Greenhouse Solar System in Tobacco Curing Mode Under Microcomputer Control (8/30-9/5, 1978).	43
12.	Solar Curing and Drying of Peanuts Showing Measured and Simulated Drying Rate.	45
13.	System Performance of Greenhouse Solar System in Grain Drying Mode Showing Solar Radiation, Inlet Air Temperature, and Measured and Simulated Outlet Air Temperatures.	46
14.	Effects of Air Flow Rate, Outside Air Temperature and Relative Humidity on Drying Time for Curing 3 Tons of Peanuts from 30% to 10% Moisture Content with Clear Day Solar Insolation in Mid-October	47

LIST OF FIGURES CONT'D

Figure		Page
15.	Simulated System Performance of Greenhouse Solar Drying System with a 6-ton Drum Unit for Solar Peanut Curing.	48
16.	Total Solar Radiation, Inlet and Outlet Air Temperatures.	50
17.	Total Solar Radiation, Inlet and Outlet Air Temperatures.	51
18.	Total Solar Radiation, Inlet and Outlet Air Temperatures.	52
19.	Total Solar Radiation, Inlet and Outlet Air Temperatures.	53
20.	Total Solar Radiation, Inlet and Outlet Air Temperatures.	54
21.	Total Solar Radiation, Inlet and Outlet Air Temperatures.	55
22.	Total Solar Radiation, Inlet and Outlet Air Temperatures.	56
23.	Efficiency Curve for Bulk-Curing/Greenhouse System.	59
24.	Cucumber Production with Containerized Soil Culture in Solar Barn.	62
25.	Tomato Production with Hydroponic Culture in Solar Barn.	62
26.	Automated Tobacco Seedling Production Systems: (a) Stationary Layer System Utilizing Portable Frames; (b) Rotary Layer System Utilizing Rotary Drums.	64
27.	Seedling Growing and Handling Tray, Tobacco Transplants Pulled out from the Tray Showing the Effect of Air Pruning on Plant Roots to Maintain Uniform Root System.	66
28.	Field Transplanting of Solar Barn Grown Tobacco Transplants Using the Two-Row Fully Automatic Transplanter.	66
29.	Growth Curves for Tobacco Plants Transplanted from Greenhouse Solar System and Conventional Plantbed.	67

LIST OF FIGURES CONT'D

Figure		Page
30.	Schematic Diagram Showing Physical Components and Analogous Circuit Elements for Greenhouse Solar Drying System.	69
31.	Thermal Circuit Simulation Model for Greenhouse Solar Drying System.	77
32.	Solar Radiation, Outside and Inside Air Temperatures, and Measured and Predicted Solar Drum Surface Temperatures.	80
33.	Simulated and Measured Temperature-Time Response of Greenhouse Solar Drying System.	82
34.	Gravel Bed Sensible Heat Storage System.	84
35.	Experimental Clear Cylindrical Latent Heat Storage Elements.	84
36.	Ring Baffled Storage Unit.	88
37.	Cross Baffled Storage Unit.	88
38.	Latent Heat Storage System with Ring Baffles: (a) Air Flow Pattern between Storage Rods; (b) Top View of Bottom Layer Rods and Ring Baffles Arrangement.	89
39.	Cross Section of Latent Heat Storage System with Ring Baffle.	90
40.	Latent Heat Storage System with Cross Baffles.	91
41.	Cross Section of Latent Heat Storage System with Cross Baffles.	92
42.	Schematics of Experimental Setup.	94
43.	Schematic of Control System.	97

LIST OF TABLES

Table		Page
1.	Energy Consumption in Tobacco Bulk Curing.	8
2.	Heat Balance Equations for System Solar Collectors.	32
3.	Daily Total Solar Radiation Incident upon Horizontal Surface and Weather Conditions.	49
4.	Temperature, Solar Radiation and System Efficiency.	58
5.	Nomenclature and Symbols.	70
6.	Thermal Properties of Materials Used.	71
7.	Units and Scale Factors of Analogous Electrical and Thermal Parameters.	71
8.	Values of Solar Collector Component Conduction Path Resistors and Capacitors.	78
9.	Convection Resistances for Solar Collector Components.	78
10.	Inside Radiation Exchange Network Resistances ($R \times 10^3$ ohms).	79
11.	Properties of Latent Heat Storage System.	85
12.	Thermo-Physical Properties of Calcium Chloride Hexahydrate.	87
13.	Net Weight of Calcium Chloride Hexahydrate in Clear Rods.	87
14.	Thermocouple Locations and Channel Number.	95

INTRODUCTION

The increasing scarcity and cost of many fuels is at present a major concern in agricultural production. This may be even more important in future years since the production of food, feed and fiber is critically dependent on adequate supplies of energy for agricultural production and for the manufacture of equipment, fertilizers and pesticides. Problems of world wide energy distribution, availability and cost have resulted in an increasingly urgent need for responsible, well-informed and effective decision making on the part of government, industry, agriculture, and the energy consumer to deal with these complex and highly important problems of energy use and conservation in agriculture.

The realization that an alternative source of fuel must be utilized became uncomfortably apparent to the American farmer who saw spiralling fuel and electric costs in recent years. Although concern about decreasing energy reserves has been a predominant issue for the past several years, only recently has its economic effects been so keenly felt. Alternatives have become necessities in the search for a replacement for fossil fuels. Solar thermal energy collected on the earth's surface without concentrating devices is essentially a low temperature heat source. This characteristic and the seasonal requirement for drying of agricultural crops makes solar energy ideally suited for low temperature drying and supplemental heating applications in agricultural production. The ultimate measure of solar energy utilization is benefits versus cost.

A solar facility that is low in the cost and can be utilized on a practical year-round basis is necessary to overcome hesitations involved in switching farm operations typically handled with fossil fuels to solar heat.

Effective year-round solar energy utilization has been realized using the greenhouse solar system developed by Huang et al. [18, 25, 26, 29, 30]. The system is a multipurpose structure which utilizes solar energy as a first priority energy source to dry farm crops such as tobacco, peanuts and grains from mid-July to November and to produce greenhouse crops and tobacco seedlings the remainder of the year. This multipurpose farm structure uses two basic approaches to the capture and storage of solar energy. First, as a curing and drying structure, it is designed to utilize physical equipment to collect, store and use solar energy to dry farm crops. Second, as a fully controlled greenhouse, solar energy is used for space heating for fuel savings and photosynthesis for maximum plant or biomass production. In the air pre-heating and energy storage arrangement, solar energy provides a definite fuel and electricity savings as an alternative, first-consumed energy source in both drying mode and greenhouse mode operations for agricultural production [2, 3, 18, 21, 25, 27, 50]. Various container and hydroponic cultures have been demonstrated for full scale production of flowers, tomatoes, cucumbers and tobacco seedlings. High germination rates of 95-97 percent and fairly uniform growth have been obtained for tobacco transplants using seedling growing and handling trays adapted to fully automatic transplanter. The three years of field growth study and the statistical analyses have shown that the effect of initial seedling size is non-significant and that the solar barn grown seedlings have resulted in significantly better growth and yield [21].

During both drying and greenhouse modes of operation, the microcomputer-based control system has been used to control the system's air flow patterns to maximize the utilization of available solar energy and control the environmental conditions within the system [41, 42, 43]. The feasibility of controlling

and monitoring the operations of the greenhouse solar system using micro-computers has been demonstrated using a simple control schedule [2]. Weather variability has been incorporated in the decision-making process as control inputs. The tests results have shown that the air circulation and flow inside the system can be controlled effectively by activating fans, vents and shutters to provide automated environmental control for air and space heating, cooling and energy storage [41, 42].

The basic concept of solar barn, using the total structure as a "multi-directional" solar collector with curing or drying chamber and storage system exterior surfaces serving as collector heat absorbers, has been adapted to conventional bulk curing box barns. The on-farm full scale tests have shown that significant fuel savings were achieved in solar bulk curing of tobacco in large containers. Analyses for the solar barn thermal behavior and efficiency as multi-directional solar collector showed that the total system efficiency was 44-55%. A latent heat storage system was designed and constructed to be used as an integrated part of solar barn to replace the sensible heat gravel energy storage system.

Circuit simulation analyses of the greenhouse solar drying system have been performed for both tobacco and peanut curing modes. Temperature predictions obtained by the thermal circuits conformed favorably to the experimental results [24, 28].

The prime objectives in developing the greenhouse solar system have been to provide: (1) an efficient solar energy utilization in agriculture to save both fossil fuels and electricity; (2) a solar system which is competitive in initial cost as compared to a conventional curing or drying unit; and (3) a multiple-use solar system which can be utilized all year for an effective farm

REPORT FOR TRAZER SYSTEM

operation. The project represents seven years of full-scale field testing for the above mentioned various modes of operation, the data acquisition and analyses, system design and optimization, as well as modeling and simulation studies. This report covers those research activities that pertain to the total system concept and design, the system operation and performance, the analysis and experimental verification, and the illustration of effective year-round solar energy utilization in agricultural production.

The system consists of a solar collector area of 7.11 million sq ft and a storage tank of 1.5 million gal capacity. The solar collector area is divided into four zones of about 1.8 million sq ft each. Each zone is equipped with a solar collector and a storage tank. The solar collector is a flat plate collector and the storage tank is a cylindrical tank.

The system has a capacity to store 1.5 million gal of water at 140°F. The system is designed to provide 100,000 gal of water per year at 140°F. The system is designed to provide 100,000 gal of water per year at 140°F.

The solar collector area is 7.11 million sq ft. The solar collector area is 7.11 million sq ft. The solar collector area is 7.11 million sq ft. The solar collector area is 7.11 million sq ft.

The solar collector area is 7.11 million sq ft. The solar collector area is 7.11 million sq ft. The solar collector area is 7.11 million sq ft. The solar collector area is 7.11 million sq ft.

The solar collector area is 7.11 million sq ft. The solar collector area is 7.11 million sq ft. The solar collector area is 7.11 million sq ft. The solar collector area is 7.11 million sq ft.

The solar collector area is 7.11 million sq ft. The solar collector area is 7.11 million sq ft. The solar collector area is 7.11 million sq ft. The solar collector area is 7.11 million sq ft.

ENERGY FOR TOBACCO CURING

Energy conservation has become one of the number one goals in both developed and developing countries. The magnitude of the problem becomes evident when we consider the size of the income and current fuel requirements for bright leaf tobacco curing. For example with an estimated 100,000 acres, and 0.2 billion pounds of cured leaf, it is estimated that one billion pounds of water must be evaporated during curing. While the theoretical energy for evaporating this quantity of water is equivalent to 7.17 million gallons of No. 2 fuel oil, actual fuel requirements are estimated to be three to four times as large, or about 25 million gallons. Major research and observations for three types of curing systems - natural convection, forced-air stick curing, and bulk curing - show the following:

1. The average heat energy for all systems was 16,400 Btu per pound, or 3.3 times the theoretical, assuming five pounds of water per pound of cured leaf.
2. Bulk curing barns used less energy (12,700 Btu per pound) on average than the other systems. Even allowing for extra fan horsepower, the bulk system gave a 14% energy reduction in comparison with the overall average.
3. The forced convection conventional barns used the most energy (17,530 Btu per pound). This was blamed in most cases to excessive exfiltration from the units.
4. The natural convection barns averaged 15,933 Btu per pound, intermediate between forced convection and bulk.

It was interesting to note that the lowest observed measurement was 7,800 Btu per pound or about 1.6 times the theoretical heat of evaporation while the largest was 29,900 Btu per pound or about 6 times the theoretical.

Fuel needs for curing burley tobacco are not as great as for flue-cured tobacco. The recommended amount of supplemental heat needed in the conventional burley barn is approximately 200,000 Btu/hr-A. Burley tobacco farmers have used as much LP gas as 300 gal/A in a two-tier forced ventilation barn.

Radiation from the sun is the source of almost all energy on earth. Agriculture, even in its most primitive form, encompasses those activities of man related to the collection and storage of solar energy in a form useful for the sustenance of life processes. Photosynthesis for food production and field drying for processing agricultural materials are two important, natural uses of solar energy.

A solar curing system for flue-cured tobacco or for burley tobacco would greatly reduce the farmer's dependence on fossil fuels as the heat source. Of equal importance is the potential for consistently curing top quality tobacco through a more controlled curing environment. The solar system needs to be kept simple and effective so that it is competitive in the initial cost as compared to a conventional curing unit. The system should ideally be multiple purpose so that it can be used all the year round for an effective solar energy utilization and farm operation.

In solar curing of flue-cured tobacco effective year-round solar energy utilization has been realized using the greenhouse solar system (solar barn) developed by Huang et al. [18, 26, 29, 30]. The fuel savings potential with this system in tobacco curing is two fold. There is a significant fuel savings associated with bulk curing alone plus the added fuel savings realizable from solar energy.

In order to compare fossil-fuel energy consumption in the greenhouse

bulk curing solar barn with other bulk curing systems, energy data is presented in Table 1 for various types of curing and types of fuel. The table only includes the on-farm full-scale curing operations, because it is very misleading to compare the results of any scale-down curing studies on energy savings with a full-scale curing. For bulk curing these figures do not include the electric energy required for air flow and circulation to cure tobacco in these barns. In general, direct fire LP curing is more efficient energy-wise than indirect fire oil curing. Also, as shown by the N.C. State University/Biological and Agricultural Engineering (NCSU/BAE) extension studies, the fuel crisis and education of tobacco farmers to bulk curing management have significantly reduced fuel consumption for some farmers (Part of this crease is attributable to yearly crop variation). As shown by Table 1, the original solar barn system and the improvements made over the past years can contribute significantly to reduce fossil fuel consumption in tobacco curing. The electricity required for the conventional bulk barn furnace fan costs almost as much as does the fuel. The solar barn auxiliary fan can substitute for the main fan during stem drying and later stage of leaf drying. It requires only one-fourth the power of the main fan.

Full-scale tobacco cures in midsummer with the U.S. solar barn at the Central Crops Research Station in Clayton (latitude $35^{\circ} 41'N$), N.C. have demonstrated quality tobacco curing with an overall 51% fuel savings as compared with a conventional bulk curing barn under the same curing management [2].

The solar barn design and concept have been adapted to the tobacco curing and culture for Asian farm conditions. The solar barn capacity is equivalent to a conventional Japanese bulk barn or about one-third of a U.S. bulk barn. Full-scale on-farm solar barn tests were conducted in midwinter at Pingtung

TABLE 1. ENERGY CONSUMPTION IN TOBACCO BULK CURING.

Bulk Curing Study	Year	Average BTU/lb of Ordered Tobacco	Low Cure or Average (BTU/lb)	Type of Cure	Type of Fuel Energy*
"Energy & U.S. Agriculture" USDA Publication		22,454		Sticks & Rack	LP, Oil, NG
Canadian Survey	1974-1975	16,400 12,695	7,754(LP)	Sticks & Rack Bulk (Rack)	LP, Oil, NG LP, Oil, NG
NCSU/BAE Extension Energy Studies of Commercial Barns	1976	21,836 11,979	15,609 10,819	Bulk(Box & Rack) Bulk(Box & Rack)	Oil LP
	1977	16,598 9,138	11,586 8,481	Bulk(Box & Rack) Bulk(Box & Rack)	Oil LP
Central Crops Res. Station Commercial Bulk Barn	1975 1976	11,327 9,776		Bulk (Rack) Bulk (Rack)	LP LP
Cross-Flow Barn Being Developed by NCSU/BAE	1975 1976	9,076 11,440	6,340	Bulk (Box) Bulk (Box)	LP** LP
Solar Barn Being*** Developed by NCSU/BAE	1975 1976 1977 1978	7,101 6,885 6,282 6,785	4,894	Bulk (Rack) Bulk (Rack) Bulk (Rack) Bulk (Rack)	LP** LP LP LP

*Types of fuel are LP-liquid petroleum, oil-fuel oil, and NG-natural gas, LP and NG heating units are direct fire, and oil is indirect fire.

**These barns only have the commercial heating units.

***Solar energy collected and utilized by solar barn was in addition to the energy figures (BTU/lb) given in table.

(latitude $22^{\circ} 44'N$), Taiwan. The results showed that the solar barn provided about 40% fuel saving over the conventional Japanese bulk curing barn [8]. Official tests conducted for the Taiwan solar barn in Philippines showed that the average BTU consumption was 20,354.77 BTU/kg cured using diesel oil [47]. The energy savings by the solar barn system was 60.46% as compared with the results of prior conventional curing studies in Philippines.

Considerable fuel savings have been obtained using roof solar collectors in conjunction with scale-down tobacco curing facilities. A cross-flow barn design with solar collector on the roof and a heat exchanger to reclaim heat from the exhaust air has been studied by Johnson [33]. He reported an average petroleum fuel efficiency for 12 cures of 8.0 MJ/kg cured, assuming 15% M.C. dry basis and 90% combustion efficiency. Tobacco curing using three single room wide units built to one-fifth of a conventional bulk barn connected to a shed roof flat plate solar collector and rock storage has been studied by Cundiff [12]. He reported that overall for the 12 cures the solar input was 6.7 MJ/kg cured and the fossil fuel supplement was 12.7 for a total of 19.4. The solar system supplied about one-third of the total heat energy required in tobacco curing. The main drawbacks of these scale-down facilities are considerably higher initial investments as compared with a conventional bulk barn and lack of year-round utilization for agricultural production.

In solar curing of burley tobacco Walton, et al. [49] proposed a two stage solar curing system to reduce the fossil fuels needed to provide the proper curing environment. The first stage is solar field curing under direct solar radiation. The second stage is to complete the cure in a solar curing facility using solar energy as the source of heat during curing. They experimentally evaluated the capabilities of the four types of forced ventilation

curing chambers; (1) conventional chamber with metal roof, (2) solar-transmitting-fiberglass-roof chamber, (3) solar-collector chamber with no heat storage capability, and (4) solar-collector-rockbed-storage chamber, to reduce high relative humidity during curing. They concluded that the average daily relative humidity was up to 5 percentage points less in all the solar energy utilizing chambers as compared to the conventional chamber. The solar-collector-rockbed-storage system was superior to other two solar systems because it provided heat during critical periods of high humidity. The solar-collector-rockbed system supplied enough heat to reduce the relative humidity from the 80-90% range to the desired 65-70% range for 3 days of rainy weather curing without replenishing. A solar burley tobacco curing facility with a 3 to 4 day heat supply stored in the rockbed should provide the capability to prevent the 6% tobacco quality loss by using solar heat to lower relative humidity.

SYSTEM DESIGN AND DESCRIPTION

The greenhouse solar system basically consists of a transparent exterior or greenhouse outer-shell which acts as the solar collector glazing and removable or interchangeable inner chambers which functions as the multi-directional heat absorbers of the solar collector. The quonset shaped structure made of tedlar coated clear corrugated fiberglass and pipe frames has dimensions of 7.6 m wide, 4.0 m high and 9.2 m long. Figures 1 (a) and (b) respectively show the tobacco bulk curing mode and grain or peanut drying mode setups. The system is equipped with an oil or gas furnace unit with temperature, humidity, air flow controls, and a gravel solar collector/energy storage system. All internal surfaces are painted black for efficient solar energy conversion and parallel corrugated slotted ducts are embedded underneath the gravel beds to ensure uniform air flow throughout the gravel for effective energy storage [18, 30, 50].

the structure is oriented North-South to allow its multi-directional collection surface to maximize solar energy collection for this latitude location ($35^{\circ} 41'N$). The crosssectional view of the structure is shown in Fig. 1 (c) illustrating the tobacco curing mode at left side of greenhouse symmetrical center line and grain drying mode at right. When the structure is not used as a curing and drying facility it can be converted to a greenhouse mode, and solar energy is then used effectively for space heating and plant photosynthesis under a controlled environment for maximum food or plant production.

Solar energy is used as a first priority energy source in all stages of tobacco curing model to supplement the energy requirement for bulk curing of tobacco. Incoming air for the furnace is preheated

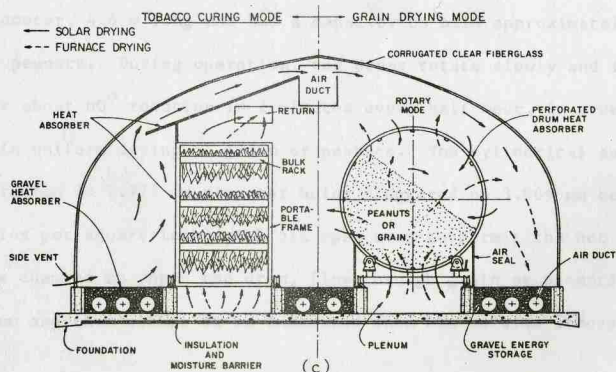
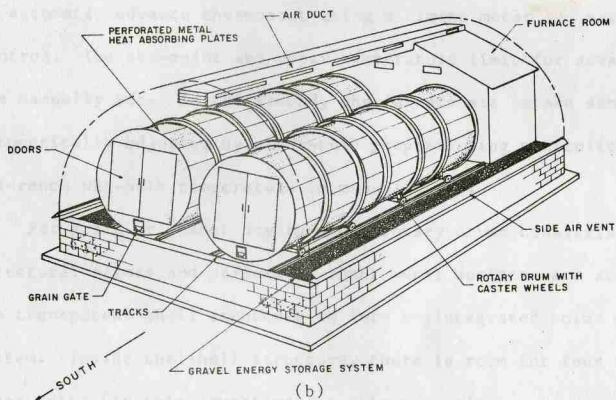
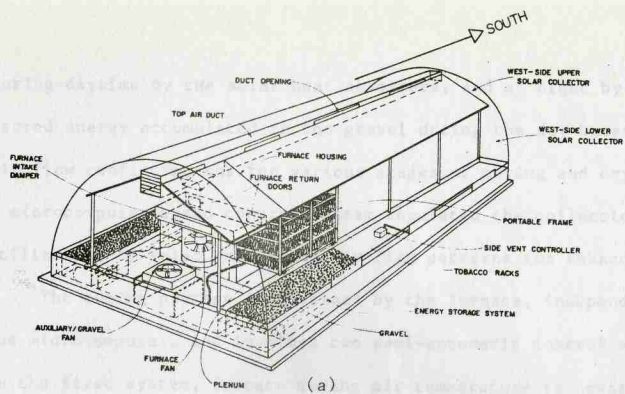


Fig. 1. Greenhouse Solar System Setup: (a) Tobacco Curing Mode; (b) Peanut Curing or Grain Drying Mode; (c) Illustration of Typical Air Flow Patterns for Solar Drying and Furnace Drying.

during daytime by the solar heat absorbers, and at night by the stored energy accumulated in the gravel during the day based on the air flow configurations for various stages of curing and drying [26]. A microcomputer-based control system regulated the collection and utilization of solar energy and air flow patterns for tobacco curing [2].

The curing process is governed by the furnace, independent of the microcomputer, and involves two semi-automatic control systems. In the first system, furnace curing air temperature is controlled by an automatic advance thermostat using a timing motor and set-point control. The set-point and upper temperature limit for advancement are manually set. In the second, the furnace air intake damper is automatically adjusted by a wet-bulb proportioning controller whose reference wet-bulb temperature is manually set.

For grain or peanut drying mode, rotary drums consisting of structural frames and perforated sheet metal surfaces are set inside the transparent shell structure to form an integrated solar collector system. Inside the shell structure, there is room for four cylindrical dryer units (in this investigation only one unit was used) each 2.2 m diameter, 4.6 m long and has a capacity to hold approximately 6 tons of peanuts. During operation, the drums rotate slowly and intermittently, or about 60° rotation in 2 minutes every half hour, in order to maintain uniform drying of grain or peanuts. The cylindrical surface perforation is 2.972 mm diameter holes staggered on 3.969 mm centers (47 holes per square inch) with 51% open area to permit the hot air from the chamber to enter the drum, flow through grain or peanuts inside the drum and then either to be exhausted into the outside atmosphere or

recirculated within the structure. The black surface of the drum also acts partly as a solar heat absorber collector, because it is heated by the absorption of solar radiation incident upon it and dissipates the heat both into the air in the structure and to the grain or peanuts. The perforation allows the dark hole effect to achieve an effective solar energy collection. It can be operated for solar or furnace drying with the drum set for rotary mode for drying grain or peanuts, or set for stationary mode with perforated shelves for dehydrating processed products.

During the daytime solar energy is continuously collected by the drum and the other internal surfaces to heat the air flowing through the material being dried. When the solar energy is minimum or not available, reverse flow furnace drying is utilized. The reverse flow furnace drying can be performed in conjunction with dehydration and waste heat recovery using the structure and gravel storage system to reduce the energy requirement. For rotary mode, periodical agitation is provided to achieve more uniform grain drying and to serve as a grain cleaner. The drum can be designed as stationary unit fixed in the transparent shell structure or as a portable unit to be set on a trailer for field loading like a conventional grain or peanut wagon. The drum is then rolled from trailer into the structure for solar energy curing and drying. During greenhouse mode of operation the rotating drums further serve as a ferris wheel plant production system and the portable frames serve as a multiple layer plant production system as shown in Fig. 2(a), enhancing the economic feasibility of the total system. Figure 2(b) shows the greenhouse mode for hydroponic culture. In addition to the gravel energy storage, the nutrient solution in the plenums acts as a heat sink for solar energy storage and environment control. Figure 3 shows the solar system adapted to conventional bulk curing barns.

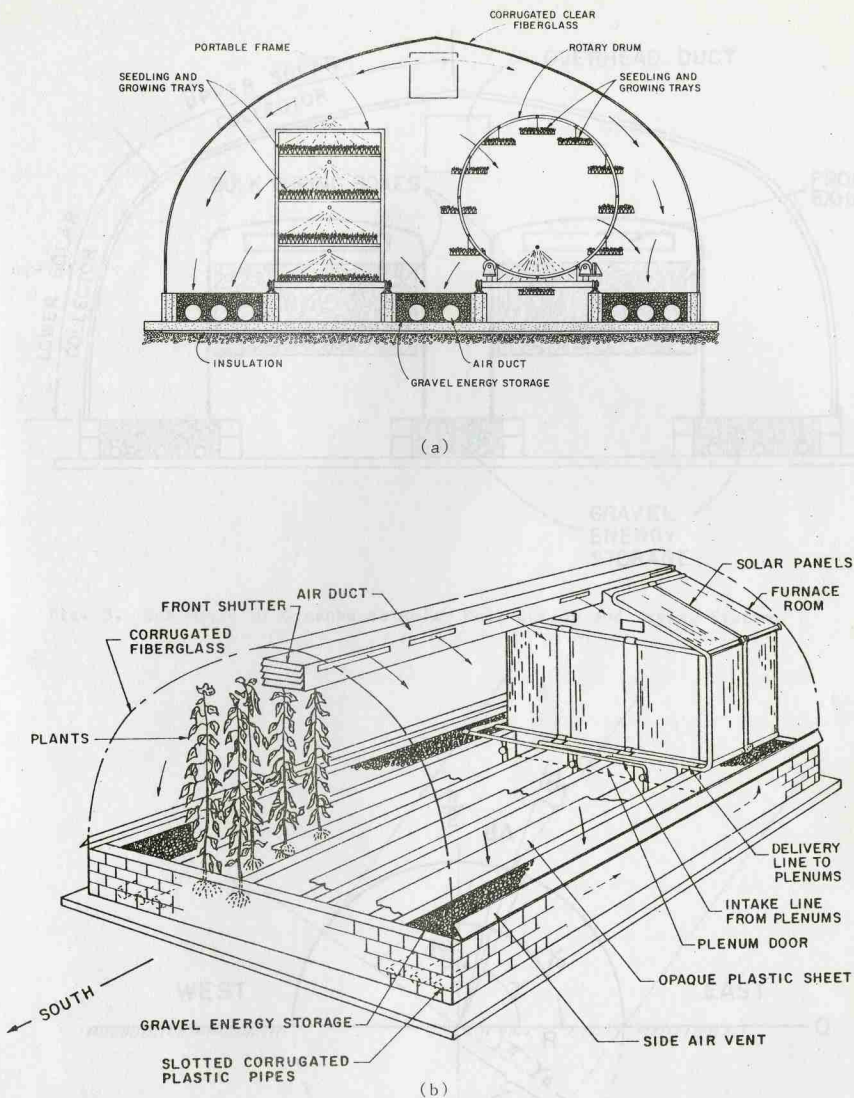


Fig. 2. Greenhouse Solar System Setup for Greenhouse Mode Showing Typical Air Flow Pattern: (a) Stationary and Rotary Layer Automated Seedling Production Systems Utilizing Portable Frames and Rotary Drums; (b) Hydroponic Plant Production with Liquid Solar Heat Collection and Storage System.

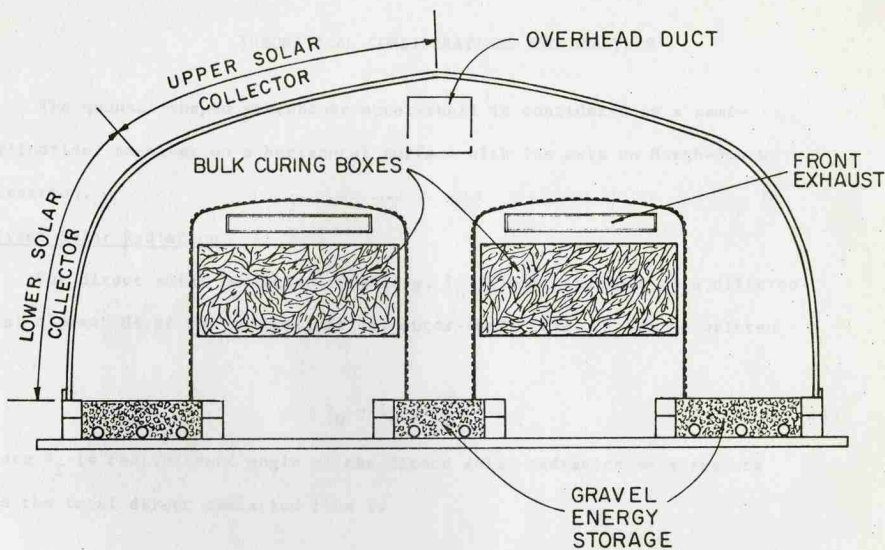


Fig. 3. Schematic of Greenhouse Solar Bulk Curing and Drying System.

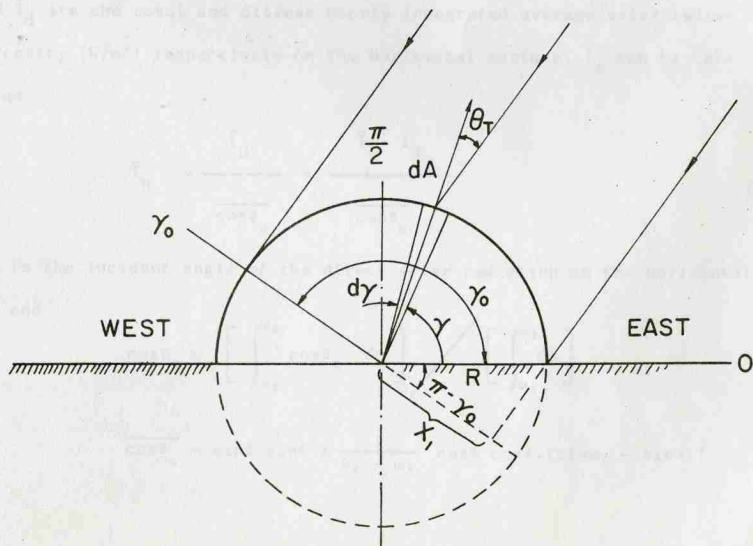


Fig. 4. Direct Solar Radiation Incident upon a Semicylindrical Receiver.

THEORETICAL CONSIDERATIONS AND ANALYSIS

The quonset shaped greenhouse outer-shell is considered as a semi-cylindrical receiver on a horizontal surface with its axis on North-South direction.

Direct Solar Radiation

The direct solar radiation intensity, I_D (W/m^2), incident on a differential element dA of the semicylindrical outer-shell (Fig. 4) can be written as

$$I_D = \bar{I}_n \cos \theta_T \quad (1)$$

where θ_T is the incident angle of the direct solar radiation on a surface and the total direct radiation flux is

$$dq_D = \bar{I}_n \cos \theta_T R L d\psi \quad (2)$$

in which R and L are the radius (m) and length (m) of the outer-shell.

If \bar{I} and \bar{I}_d are the total and diffuse hourly integrated average solar radiation intensity (W/m^2) respectively on the horizontal surface, \bar{I}_n can be calculated as

$$\bar{I}_n = \frac{\bar{I}_D}{\overline{\cos \theta_z}} = \frac{\bar{I} - \bar{I}_d}{\overline{\cos \theta_z}} \quad (3)$$

where θ_z is the incident angle of the direct solar radiation on the horizontal surface, and

$$\overline{\cos \theta_z} = \left[\int_{\omega_1}^{\omega_2} \cos \theta_z d\omega \right] / \left[\int_{\omega_1}^{\omega_2} d\omega \right] \quad (4)$$

$$\overline{\cos \theta_z} = \sin \delta \sin l + \frac{1}{\omega_2 - \omega_1} \cos \delta \cos l (\sin \omega_2 - \sin \omega_1) \quad (5)$$

in which δ is declination, l is latitude, and ω is hour angle. The azimuth angle γ is $+90^\circ$ for the east faced and -90° for the west faced surfaces on the semicylindrical receiver along the North-South direction. With these azimuth angle, incident angle θ_T of the direct solar radiation incident on a tilted surface can be written as [13],

$$\begin{aligned} \cos\theta_T = & \sin\delta \sin l \cos\phi - \sin\delta \cos l \sin\phi \cos\gamma \\ & + \cos\delta \cos l \cos\phi \cos\omega \\ & + \cos\delta \sin l \sin\phi \cos\gamma \cos\omega \\ & + \cos\delta \sin\phi \sin\gamma \sin\omega \end{aligned} \quad (6)$$

where ϕ is tilt angle. By introducing

$$\gamma = +90^\circ \text{ and } \gamma = -90^\circ \quad (7)$$

we can find

$$\begin{aligned} \cos\theta_T = & \sin\delta \sin l \cos\phi + \cos\delta \cos l \cos\phi \cos\omega \\ & - \cos\delta \sin\phi \sin\omega \end{aligned} \quad (8)$$

where the minus and plus signs are for the west and east faced quarters of the semicylindrical receiver. Therefore dq_D can be written as

$$dq_D = \frac{\bar{I} - \bar{I}_d}{\cos\theta_z} \cos\theta_T dA = \frac{\bar{I} - \bar{I}_d}{\cos\theta_z} \cos\theta_T R L d\psi \quad (9)$$

The projection area of the semicylindrical surface (Fig. 4) on the plan normal to the direction of the direct solar radiation is

$$(R + x_1) L_1 \quad (10)$$

and the direct solar radiation incident upon the semicylindrical surface is equal to the radiation incident upon this imaginary surface.

By replacing x_1 with

$$x_1 = R \cos(\pi - \psi_0) = -R \cos\psi_0 \quad (11)$$

this imaginary area can be written as

$$(R + x_1) L = (1 - \cos\psi_0) R L \quad (12)$$

where

$$\psi_0 = 180 - \text{Arctan} \left[\frac{\cos\delta \sin\omega}{\sin\delta \sin l + \cos\delta \cos l \cos\omega} \right] \quad (13)$$

and it depends on time with ω . The plane of the area of $(R + x_1) L$ have an angle $(\pi - \psi_0)$ with the horizontal surface. By taking $\gamma = +90^\circ$ and $\gamma = -90^\circ$ for the morning and the afternoon respectively, incident angle for this surface can be calculated by

$$\cos\theta_T = -(q_1 + q_2 \cos\omega) \cos\psi_0 + q_3 \sin\psi_0 \sin\omega \quad (14)$$

where

$$q_1 = \sin\delta \sin l \quad (15)$$

$$q_2 = \cos\delta \cos l \quad (16)$$

$$q_3 = \cos\delta \quad (17)$$

in which (+) for the morning and (-) for the afternoon.

The total direct solar radiation incident on the imaginary surface in time interval, $\Delta t = t_2 - t_1$, is

$$Q_D = \int_{t_1}^{t_2} q_D dt \quad (18)$$

In this integral, integrant is complex function of the time and hour angle

ω . Because of the complexity, this integral has been calculated for the constant $\cos\theta_T$ with its average value at the middle of time interval. Therefore integral becomes

$$Q_D = \int_{t_1}^{t_2} q_D dt = \frac{\bar{I} - \bar{I}_d}{\cos \theta_z} R L (1 - \cos \psi_0) \left[-(q_1 + q_2 \cos \omega) \cos \psi_0 + q_3 \sin \psi_0 \sin \omega \right] \Delta t \quad (19)$$

This is an implicit expression for the total direct solar radiation incident on the greenhouse solar system in the time interval Δt .

Diffuse Solar Radiation

The total diffuse solar radiation incident on a cylindrical surface is

$$q_d = \int_0^{2\pi} [A (1 - \cos \psi) + B (1 + \cos \psi)] d\psi \quad (20)$$

The total diffuse solar radiation incident upon a semicylindrical surface (Fig. 5) can be calculated by this integral by changing its interval to $0 \sim \pi/2$, then

$$q_d = \pi(A + B) \quad (21)$$

and

$$Q_d = \pi (A + B) \Delta t \quad (22)$$

where

$$A = \frac{1}{2} \bar{I}_d R L \quad (23)$$

$$B = A \frac{\bar{I}}{\bar{I}_d} \rho_g \quad (24)$$

ρ_g = ground reflectivity

Total Radiation Incident Upon the Plane Surfaces Toward South and North

The total solar radiation intensity on a inclined plane is given as [13],

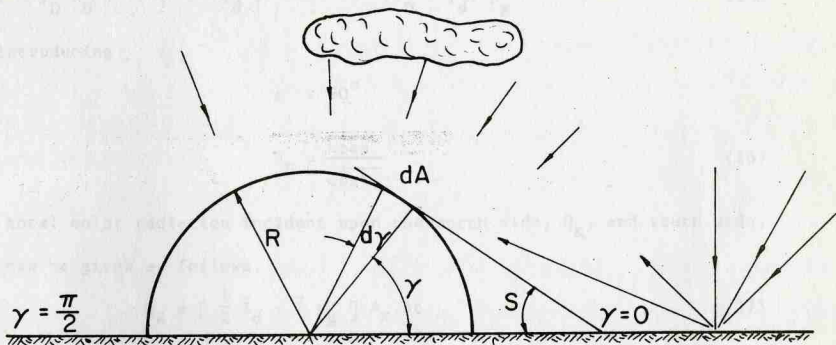


Fig. 5. Incident Diffuse Radiation Scattered by Sky and Reflected by Ground on a Semicylindrical Receiver.

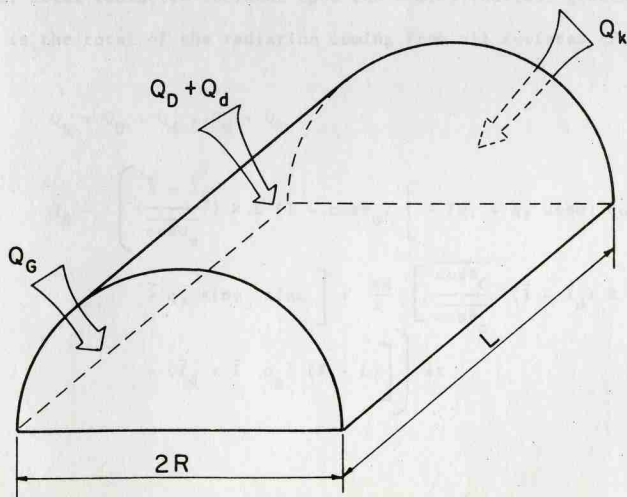


Fig. 6. Incident Solar Radiation on a Semicylindrical Receiver.

$$I = I_D R_D + \frac{1 + \cos\phi}{2} I_d + \frac{1 - \cos\phi}{2} (I_D + I_d) \rho_g \quad (25)$$

By introducing

$$\phi = 90^\circ$$

and

$$R_D = \frac{\overline{\cos\theta}}{\overline{\cos\theta_z}} \quad (26)$$

the total solar radiation incident upon the north side, Q_K , and south side, Q_G , can be given as follows,

$$Q_K = \left[\frac{1}{2} \bar{I}_d + \bar{I} \rho_g \right] A_K \Delta t \quad (27)$$

$$Q_G = \left[\bar{I} \left(\frac{\overline{\cos\theta_G}}{\overline{\cos\theta_z}} + \frac{1}{2} \rho_g \right) + \bar{I}_d \left(\frac{1}{2} - \frac{\overline{\cos\theta_G}}{\overline{\cos\theta_z}} \right) \right] A_G \Delta t \quad (28)$$

where

$$A_K = A_G = \frac{\pi R^2}{2} \quad (29)$$

Total Solar Radiation

The total solar radiation incident upon the semicylindrical greenhouse solar system is the total of the radiation coming from all surfaces (Fig. 6).

Therefore,

$$Q_S = Q_D + Q_d + Q_G + Q_K$$

$$Q_S = \left(\frac{\bar{I} - \bar{I}_d}{\overline{\cos\theta_z}} \right) R L (1 - \cos\psi_o) \left[- (q_1 + q_2 \cos\omega) \cos\psi_o + q_3 \sin\psi_o \sin\omega \right] + \frac{\pi R}{2} \left[\frac{\overline{\cos\theta_G}}{\overline{\cos\theta_z}} (\bar{I} - \bar{I}_d) R + (\bar{I}_d + \bar{I} \rho_g) (R + L) \right] \Delta t \quad (30)$$

System Efficiency

In more conventional form, the efficiency of the solar collectors have been illustrated on the $\eta - \xi^*$ coordinates system where η is taken as the efficiency and ξ^* is the variable defined as below [16],

$$\xi^* = \frac{(T_1 + T_2)/2 - T_\infty}{I} \quad (31)$$

where T_1 and T_2 are the air temperatures at inlet and outlet. For the greenhouse solar system, inlet temperature of the working fluid or air is equal to ambient air temperature during open-loop air flow configuration,

$$T_1 = T_\infty \quad (32)$$

Therefore, ξ^* given in Eq. (31) can be redefined as ξ

$$\xi = \frac{T_2 - T_\infty}{I} \quad (33)$$

The efficiency, η , has been defined as [16],

$$\eta = \frac{Q_u/A}{I} \quad (34)$$

for the flat-plate and concentrating solar collectors, in which Q_u is the useful energy collected by the collector with collector area A , and I is the total solar energy incident upon the solar collector per unit time and per unit area.

In this study, two kinds of efficiency have been defined for the greenhouse solar system. The first one is the "instantaneous efficiency" or the "short term efficiency" which can be calculated by using Eq. (34). However, in this case a new definition has to be introduced for the total solar energy flux incident upon greenhouse solar system rather than the product $(A I)$. In this

situation η can be defined as;

$$\eta = \frac{Q_u}{Q_s} \quad (35)$$

where Q_s is the total solar energy flux incident upon the greenhouse solar system.

The second definition of the efficiency has been derived by integrating Eq. (35) over the day and called the daily efficiency,

$$\eta_d = \frac{\int_d Q_u dt}{\int_d Q_s dt} \quad (36)$$

A part of solar energy incident upon the greenhouse solar system is stored in the component of the system as a sensible heat by rising their temperature. The rest of energy is stored in the circulating air. During nighttime part of the stored energy in the structure is given back to the circulating air. Therefore, the integration of the Q_u over the day gives the chance of computing this stored energy as a part of the useful energy, and the total efficiency can be then calculated. Short term efficiency can be shown on the $\eta - \xi$ axis. But for the daily efficiency a new ξ_d axis has been defined as

$$\xi_d = \frac{\bar{T}_2 - \bar{T}}{\bar{I}} \quad (37)$$

where \bar{I} , \bar{T}_2 and \bar{T} indicates the daily average values.

The bulk-curing/greenhouse system or solar barn has a North-South orientation, hence there is an East and West collector storage system. East collector storage system has its peak temperature in the morning hours and the West collector storage system peaks in the afternoon hours. Under steady state conditions the effective useful energy stored in the gravel beds can be estimated with Eq. (38) and data for collector exit air and gravel bed exit air temperatures.

$$Q_e = V_a \rho C_{pa} t \Delta T_a \quad (38)$$

where

Q_e = stored energy (J)

V_a = air flow rate (m^3/hr)

ρ = density of air ($1.07 \text{ kg}/m^3$)

C_{pa} = specific heat of air ($\text{kJ}/\text{kg}^\circ\text{C}$)

t = duration (hr)

ΔT_a = change in air temperature ($^\circ\text{C}$)

The above described greenhouse solar system is basically a large solar collector in which the curing and drying process is taking place as the system is set for curing and drying mode. The process involves utilization of solar energy to heat the atmospheric air and utilization of the heated air to cure and dry agricultural crops. During the process there are four system components; (a) outer and inner heat transfer surfaces, (b) working fluid or air, (c) heat storage media, and (d) agricultural crops, affecting the heat and mass transfer of the system. Different drying equipments and air flow patterns require different approaches for the heat and mass transfer analysis.

Solar Heating of the Air

Several assumptions are made for the quasi steady-state heat transfer analysis of the system. Heat capacity of the structural

elements and conductive heat losses through the floor to the ground are neglected. The thermal properties of elements are constant. Only convective and radiative heat transfer are considered between heat transfer surfaces and the air.

1. Solar Grain or Peanut Drying: The basic analysis was performed for curing and drying of peanuts [45]. In the analysis the surface area of the fiberglass shell is divided into several plane sections, comprising two end surfaces and five sections for the quonset shaped surface. The steady-state energy balance equation for the shell surface is

$$\left[h_{ocj} + h_{ij} + h_{orj} + \sum_{k=1}^N h_{rjk} \right] \Delta T_j - \sum_{k=1}^N h_{rjk} \Delta T_k - \frac{1}{2} h_{ij} \Delta T_a = q_j + R_j \quad (39)$$

where q = solar heat flux (W)

h_i, h_{oc} = convective heat transfer coefficient for inside and outside surfaces, respectively ($W/m^2 \text{ } ^\circ C$)

h_r, h_{or} = radiative heat transfer coefficient for inside and outside surfaces, respectively ($W/m^2 \text{ } ^\circ C$)

T = temperature ($^\circ C$)

T_∞ = outside temperature ($^\circ C$)

$\Delta T = T - T_\infty$ temperature difference ($^\circ C$)

$R_j \approx h_{orj} (T - T_{sky})$

T_{sky} = sky temperature ($^\circ C$)

$j = 1, 2, \dots, M$ with $M = 7$ is the total number of sections over the surface of the fiberglass shell.

Consider the case with one solar drum in the structure, the equation for the drum and floor surface is

$$\left[h_{ij} + \sum_{k=1}^N h_{rjk} \right] \Delta T_j - \sum_{k=1}^N h_{rjk} \Delta T_k - \frac{1}{2} h_{ij} \Delta T_a = q_j \quad (40)$$

where $j = M + 1, M + 2, \dots, N$ with $N = 14$ is the number of subdivisions for the floor and drum surfaces.

The equation for the air mass in the greenhouse is

$$\sum_{j=1}^N h_{ij} A_j \Delta T_j - \left[\frac{1}{2} \sum_{j=1}^N h_{ij} A_j + V_a \rho C_{pa} \right] \Delta T_a = 0 \quad (41)$$

where

A = area (m^2)

V_a = air flow rate (m^3/hr)

ρ = density (kg/m^3)

C_{pa} = specific heat of air ($kJ/kg^{\circ}C$)

Using the equation for the solar radiation flux for a tilted surface [13];

$$\begin{aligned} \bar{q}_s = I_D \frac{\cos \theta_T}{\cos \theta_Z} + I_d \frac{1 + \cos \phi}{2} \\ + (I_D + I_d) \frac{1 - \cos \phi}{2} \rho_g \end{aligned} \quad (42)$$

where

\bar{q}_s = average solar radiation flux for a tilted surface (W/m^2)

I_D, I_d = direct and diffuse solar radiation intensity, respectively (W/m)

θ_T, θ_Z = angle between beam component and normal to tilted and horizontal surfaces, respectively

ϕ = tilt angle of the surface from the horizontal

ρ_g = ground reflectivity

The solar radiation gain of the outer or cover surfaces can be written as:

$$q_j = \bar{q}_s \alpha_c, \quad j = 1, 2, \dots, M \quad (43)$$

and for the inner surfaces as

$$q_j = \bar{q}_s \tau_c \alpha_j, \quad j = M + 1, M + 2, \dots, N \quad (44)$$

where

α_c = cover absorbtivity

τ_c = cover transmittance

α_j = surface absorbtivity

In case of q_j on the cylindrical surface of the drum, an equivalent expression was derived by integrating Eq. (44) over the cylindrical surface. The bulk temperature of the air inside the chamber is determined from a simultaneous solution of the above system of 15 algebraic equations.

2. Solar Tobacco Curing: In the heat transfer analysis of tobacco curing mode only one equation is written for all heat transfer surfaces including cover and absorber surfaces by combining the equations written for grain drying using different factors for various surfaces. For a surface j the heat balance equation can be expressed as summation of solar heat gain, q_{sj} , convective heat transfer between element and ambient air, q_{cj} , and radiative heat transfer between elements and their surrounding, q_{rj} , is zero.

$$q_{sj} + q_{cj} + q_{rj} = 0 \quad (45)$$

$$q_{sj} = \left[I_D \frac{\cos \theta_T}{\cos \theta_Z} \tau_{shj}^D + I_d \frac{1 + \cos \phi_j}{2} \tau_{shj}^d + (I_D + I_d) \frac{1 - \cos \phi_j}{2} \rho_g \tau_{shj}^T \right] \alpha_j \tau_j, \quad j = 1, 2, \dots, M \quad (46)$$

where

τ_{shj}^D = shade factor for direct solar radiation which is function of time

τ_{shj}^d = shade factor for diffuse solar radiation

τ_{shj}^T = shade factor for total radiation reflected by ground

and

$$q_{cj} = h_{oj} F_{jsky} (T_j - T_\infty) + h_{ij} (T_j - T_{aj}) \quad (47)$$

$$q_{rj} = q_{rj}^{sky} + q_{rj}^{int} \quad (48)$$

where

$$q_{rj}^{sky} = h_{orj} \Delta T_{sky} + h_{orj} (T_j - T_\infty) \quad (49)$$

$$q_{rj}^{int} = \sum_{m=1}^N h_{rjm} (T_j - T_m) \quad (50)$$

$$h_{orj} = 4 F_{jsky} \sigma \epsilon_j \bar{T}_{sky}^3$$

$$\bar{T}_{sky} = (T_{sky} + T_j)/2$$

$$\bar{T}_{sky} = T_\infty - \Delta T_{sky}$$

$$\tau_j = 1 \text{ and } F_{jsky} = \frac{1}{2}(1 + \cos\phi) \text{ for outer or cover surfaces}$$

$$\tau_j = \tau_c \text{ and } F_{jsky} = 0 \text{ for inner surfaces}$$

$$h_{rjm} = 4\sigma \epsilon_j \epsilon_m F_{jm} T_m^3 \text{ and } T_m = (T_j + T_m)/2$$

σ = Stefan-Boltzmann constant

ϵ = emittance

Substitute Eqs. (47), (48), (49) and (50) into Eq. (45), we obtain

$$E_j T_j - \sum_{m=1}^N h_{rjm} T_m - h_{ij} T_{aj} = L_j,$$

$$j = 1, 2, \dots, N \quad (51)$$

where

$$E_j = h_{oj}^{\text{sky}} + h_{ij} + h_{orj} + \sum_{m=1}^N h_{rjm}$$

$$L_j = (h_{oj}^{\text{sky}} + h_{orj}) T_{\infty} - q_{sj} - M_j$$

Equation (51) gives N simultaneous algebraic equations for N unknown surface temperature, T_j , and four unknown collector air temperature, T_{aj} . There are two sets of energy balance equations depending on opening or closing of side air vents.

When the side vents are open, the air flows from side vents through lower and upper collectors to the top air duct, and the heat balance equations for the air can be written as;

$$\begin{matrix} \text{EL} \\ \Sigma h_{im} A_m T_m - K_{EL} T_{aEL} = M_{EL} T_{\infty} \end{matrix} \quad (52)$$

$$\begin{matrix} \text{EU} \\ \Sigma h_{im} A_m T_m - K_{EU} T_{aEU} - M_{EU} T_{aEL} = 0 \end{matrix} \quad (53)$$

$$\begin{matrix} \text{WL} \\ \Sigma h_{im} A_m T_m - K_{WL} T_{aWL} = M_{WL} T_{\infty} \end{matrix} \quad (54)$$

$$\begin{matrix} \text{WU} \\ \Sigma h_{im} A_m T_m - K_{WU} T_{aWU} - M_{WU} T_{aWU} = 0 \end{matrix} \quad (55)$$

where

$$K_p = \frac{1}{2} \Sigma h_{im} A_m + D_p$$

$$M_p = \frac{1}{2} \Sigma h_{im} A_m - D_p$$

$$D_p = V_{ap} \rho C_p a$$

V_{ap} = air flow rate in collector p

p = EL (east lower), EU (east upper), WL (west lower), WU (west upper)

When the side vents are closed the heat balance equations for the

air can be written as;

$$\Delta t \Sigma h_{im} A_m T_m - N_p T_{ap} = A_p T_{ap}^{\text{in}} \quad (56)$$

where

$$N_p = \frac{1}{2} \Delta t \sum_{im}^p h_{im} A_m + d_p$$

$$A_p = \frac{1}{2} \Delta t \sum_{im}^p h_{im} A_m - d_p$$

$$d_p = V_p \rho C_{pa}$$

V_p = volume of air in p^{th} collector

By combining Eqs. (51), (52), (53), (54), (55) and (56) we can write $(N + 4)$ simultaneous algebraic equations for the three modes of air flow created by opening and closing of side vents and $(N + 4)$ unknown temperatures can be predicted using equations given in Table 2. The quasi steady-state temperature distribution inside the greenhouse solar system during the day can be obtained by solving the system equations. The top duct air temperature then can be calculated using the equation

$$T_a = (D_E T_{aEU} + D_W T_{aWU}) / (D_E + D_W) \quad (57)$$

*P.P. 125-127
Energy in Agric*

Heat and Mass Transfer of Drying

The drying or dehydration process occurs as the heated air passing through the agricultural crops, products, or materials to be dried. The mass balance can be expressed as the moisture loss of the material is the moisture gain of the drying air. The dynamic balance of the moisture diffusion from drying material and the drying potential of the air define the drying rate and time.

The governing equations include a gross mass balance equation for moisture loss from the drying material into the air stream, given by

$$-m_d \frac{dM(t)}{dt} = m_a^* (W_e - W_a) \quad (58)$$

TABLE 2. HEAT BALANCE EQUATIONS FOR SYSTEM SOLAR COLLECTORS.

 East vents open and west vents closed

$$E_j T_j - \sum_{m=1}^N h_{rjm} T_m - h_{ij} T_{aj} = L_j, \quad j = 1, \dots, N$$

$$EL \quad \sum_m h_{im} A_m T_m - K_{EL} T_{aEL} = M_{EL} T_{\infty}$$

$$EU \quad \sum_m h_{im} A_m T_m - K_{EU} T_{aEU} - M_{EU} T_{aEU} = 0$$

$$\Delta t \quad \sum_m h_{im} A_m T_m - N_{WL} T_{aWL} = A_{WL} T_{aWL}^{in}$$

$$WU \quad \Delta t \quad \sum_m h_{im} A_m T_m - N_{WU} T_{aWU} = A_{WU} T_{aWU}^{in}$$

Both east and west vents open

$$E_j T_j - \sum_{m=1}^N h_{rjm} T_m - h_{ij} T_{aj} = L_j, \quad j = 1, \dots, N$$

$$EL \quad \sum_m h_{im} A_m T_m - K_{EL} T_{aEL} = M_{EL} T_{\infty}$$

$$EU \quad \sum_m h_{im} A_m T_m - K_{EU} T_{aEU} - M_{EU} T_{aEU} = 0$$

$$WL \quad \sum_m h_{im} A_m T_m - K_{WL} T_{aWL} = M_{WL} T_{\infty}$$

$$WU \quad \sum_m h_{im} A_m T_m - K_{WU} T_{aWU} - M_{WU} T_{aWU} = 0$$

East vents closed and west vents open

$$E_j T_j - \sum_{m=1}^N h_{rjm} T_m - h_{ij} T_{aj} = L_j, \quad j = 1, \dots, N$$

$$\Delta t \quad \sum_m h_{im} A_m T_m - N_{EL} T_{aEL} = A_{EL} T_{aEL}^{in}$$

$$EU \quad \Delta t \quad \sum_m h_{im} A_m T_m - N_{EU} T_{aEU} = A_{EU} T_{aEU}^{in}$$

$$WL \quad \Delta t \quad \sum_m h_{im} A_m T_m - K_{WL} T_{aWL} = M_{WL} T_{\infty}$$

$$WU \quad \Delta t \quad \sum_m h_{im} A_m T_m - K_{WU} T_{aWU} - M_{WU} T_{aWU} = 0$$

where

\dot{m}_a = air flow rate (kg/hr)

m_d = total weight of the drying material (kg)

$M(t)$ = average moisture content of the drying material, dry basis (%)

W_a, W_e = specific humidity of air at inlet to and exhaust from the drying chamber (kg/kg)

The equation governing the vapor diffusion in the drying material can be written as

$$\frac{M(t) - M_{eq}}{M_o - M_{eq}} = S \quad (59)$$

where

M_o = initial moisture content of drying material, dry basis (%)

M_{eq} = equilibrium moisture content, dry basis (%)

S = solution of a parabolic diffusion equation with experimentally determined coefficient

The expression for the vapor loss by diffusion through the graniferous materials, such as peanuts, to the air is given as [51],

$$S_{peanut} = \sum_{n=1}^{\infty} \frac{4}{\gamma_n^2} \exp \left[- \frac{\kappa_1 \gamma_n^2}{\pi^2} t \right] \quad (60)$$

In which γ_n 's are the eigenvalues and κ_1 is an experimentally determined coefficient defined as $\kappa_1 = \Gamma \pi^2 / \xi^2$, with Γ the diffusion coefficient, ξ the characteristic dimension, and t is time.

Similar expression for the moisture movement in the hygroscopic foliar materials, such as the lamina of tobacco leaf, is given for the first phase of falling-rate period as [9],

$$S_{tobacco_1} = \sum_{n=1}^{\infty} \frac{2\pi^2}{\gamma_n^2 (\gamma_n^2 + \pi^2 + \pi)} \exp \left[- \frac{\Gamma \gamma_n^2}{v} t \right] \quad (61)$$

γ_n = eigenvalues or positive roots of the equation
$$\gamma_n \tan \gamma_n = \Pi$$

$\Pi = \sqrt{\Omega/\Gamma}$, a dimensionless parameter

∇ = half thickness of lamina

Ω = surface emissivity

Γ = diffusion coefficient

The second phase of falling-rate period is derived from an experimental expression as

$$S_{\text{tobacco}_2} = \left[1 - \frac{(1-n)\mu t}{(M_o - M_{eq})^{1-n}} \right]^{\frac{1}{1-n}} \quad (62)$$

where

n = reaction order, a function of relative humidity

μ = rate constant, a function of temperature

Assuming that the drying process is adiabatic and the enthalpy and wet bulb temperature remain constant during the drying, then the enthalpy H_o of inlet air is equal to that of exhaust, and the enthalpy of the moist air can be expressed as

$$H = C_{pa} T + W(C_{pw} T + A_w) \quad (63)$$

where

H = enthalpy (kJ/kg)

C_{pw} = specific heat of vapor (kJ/kg°C)

A_w = latent heat of water evaporation (kJ/kg)

Assuming that the specific heat of air and water vapor does not change much in the temperature ranges encountered during drying, we substitute the numerical values into Eq. (50) to obtain

$$1.005 T_a + W_a (1.82 T_a + 2501) = 1.005 T_e + W_e (1.82 T_e + 2501) \quad (64)$$

Thus, Eqs. (57), (58) and (64) provide three relations for the determination of moisture content of material, $M(t)$, exhaust air temperature T_e and specific humidity W_e .

Dynamic System Analysis

The furnace drying characteristics of the solar barn have been analyzed using the three most common performance criteria for analyzing system dynamic characteristics based on step type inputs:

1. The maximum (peak) overshoot: This is commonly expressed in terms of a percentage of the steady-state output.
2. The initial speed of the response: This criterion can be described by one or more of the following indices:
 - (a) Delay Time (T_D): This is the time required for the response to reach 50% of the final value.
 - (b) Rise Time (T_R): This is the time required for the response to rise from 10% to 90% of the final value.
 - (c) Settling Time (T_S): This is the time required for the response to reach and remain within a certain tolerance band (usually 2% to 5%) of its final value.
3. The Steady-state accuracy: This criterion is specified in terms of the steady-state error (E_{SS}), which is the difference between the desired output and actual output after all the transients have died out.

MICROCOMPUTER DATA ACQUISITION AND CONTROL SYSTEM

The data acquisition and control system uses a modular, M-series micro-computer originally developed by Lawrence Livermore Laboratories. This microcomputer is an 8-bit machine incorporating the Intel 8080 microprocessor chip as its central processing unit. Features of the system include a real-time clock, eight priority interrupt lines, data input interface, teletype input and output, control interface and power-down battery back-up. These features are shown functionally in Fig. 7.

The real-time clock utilizes a 60 Hz crystal oscillator which generates output pulses to interrupt the system. Every one minute, an interrupt service routine updates real-time maintained in software. Elapse times programmed within software determine execution of data acquisition and solar curing control programs. Control data point scanning and appropriate operational changes are programmed to occur more frequently than overall data scans and printouts.

The data input interface processes analog signals for input to the microcomputers [43]. There are 48 channels for determining temperature from type T thermocouples referenced to an ice bath. Additionally, 16 channels are available to record various other analog signals to monitor environmental conditions such as solar radiation, wind speed and direction, fuel consumption, etc. These 64 input channels are sequentially addressed, multiplexed and amplified appropriately for input to the 0-10 volt analog to digital converter. The multiplexing is accomplished through a series of latches, 1 out of 16 decoders and reed relays. Common output lines from each of the multiplexing networks provide signals through appropriate amplification and modification circuitry to the A/D converter. The micro-computer processes these data for updates of both data acquisition and

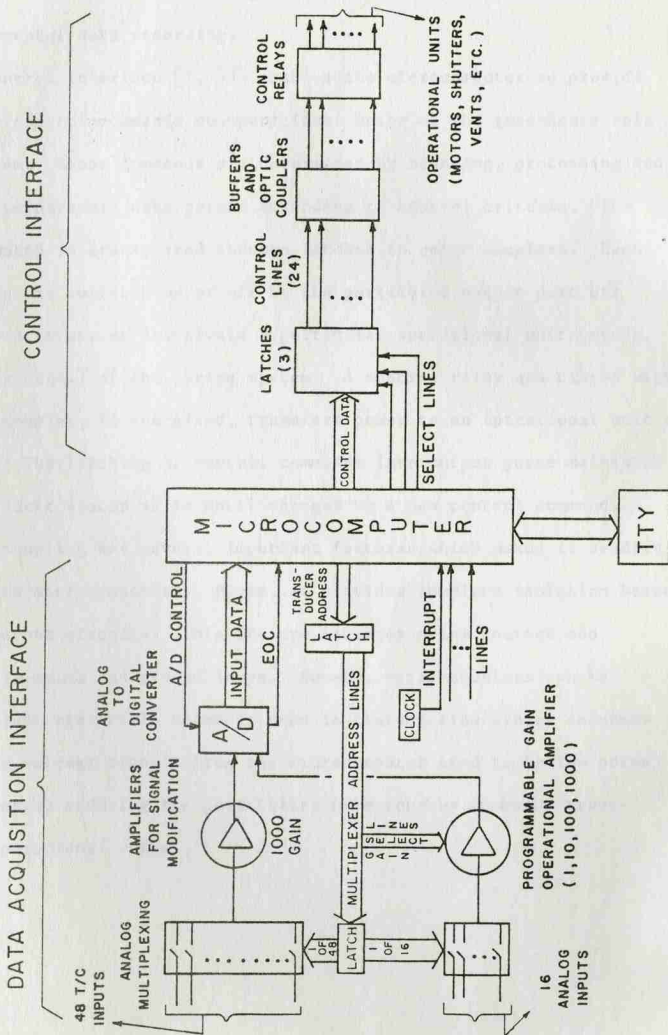


Fig. 7. Functional Description of Microcomputer Based Control System.

control status. Data and control status changes are printed via a teletype for each operational change and periodically for temperature and environmental data recording.

The control interface [2, 43] enables the microcomputer to provide appropriate control commands to operational units of the greenhouse solar curing system. These commands are determined by scanning, processing and evaluating temperature data points according to control criteria. The control command is transferred through latches to optic couplers. Each optic coupler is switched on or off by the particular output port bit reserved to activate or deactivate a particular operational unit (motor, fan, shutter, etc.) of the curing system. A control relay associated with each optic coupler, if energized, transfers power to an operational unit of the system. The latching of control commands into output ports maintains operational unit status as is until changed by a new control command.

Optic coupling has several important features which makes it readily applicable to microcomputers. First, it provides complete isolation between input and output circuits. This feature isolates noise sources and eliminates feedback and ground loops. Second, optic couplers can be switched by voltage levels commonly used in transmitting binary information. These voltage signals from the microcomputer tend to be low noise signals, thereby reducing the possibility of erroneous commands transmitted to operational units.

FIELD TEST RESULTS AND DISCUSSION

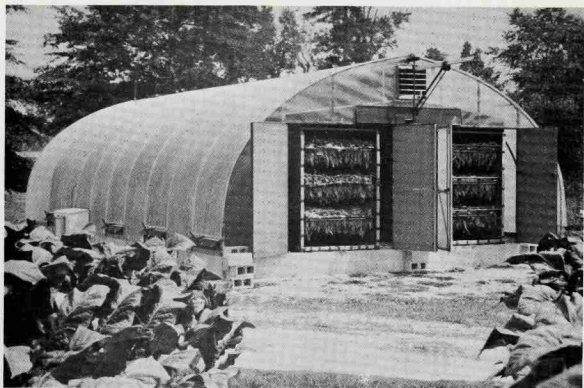
Two greenhouse solar system facilities were constructed. One unit is located at the Central Crops Research Station in Clayton, N.C. and other unit is at the North Carolina State University campus in Raleigh, N.C. The greenhouse solar system is a large multi-directional solar collector. The heating and drying processes are performed within the collector and effective solar energy utilization and system performance depend upon various air flow patterns. Therefore, the system design and performance study should be centered on a means to achieve a system control which provides adequate environmental conditions for various modes of operation.

Curing and Drying Mode Operations

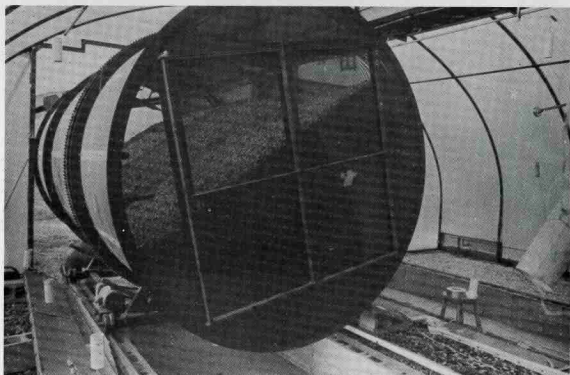
Figures 8 (a) and (b) respectively illustrate the full-scale field testing of solar curing of tobacco and peanuts at the Central Crop Research Station.

Fossil-fuel energy consumption for tobacco bulk rack curing in the solar barn is summarized in Table 1. For the first time, the tobacco bulk curing has been successfully performed under microcomputer control [2]. Figures 9 and 10 respectively show the flow charts used for yellowing and first day leaf drying and for the remaining leaf drying and stem drying.

Typical data for microcomputer controlled solar bulk curing of tobacco have been plotted as shown in Fig. 11. The temperature difference between preheated and outside air temperatures represents the degree of controlled solar energy management by the system in relation to curing air requirements to obtain quality curing which include biophysical interaction. The difference between the set point and the preheated air temperatures is indicative of the energy which the furnace had to supply to meet the desired curing schedule. The air temperature



(a)



(b)

Fig. 8. Field Operation of Greenhouse Solar System: (a) Tobacco Curing Mode; (b) Peanut Curing or Grain Drying Mode.

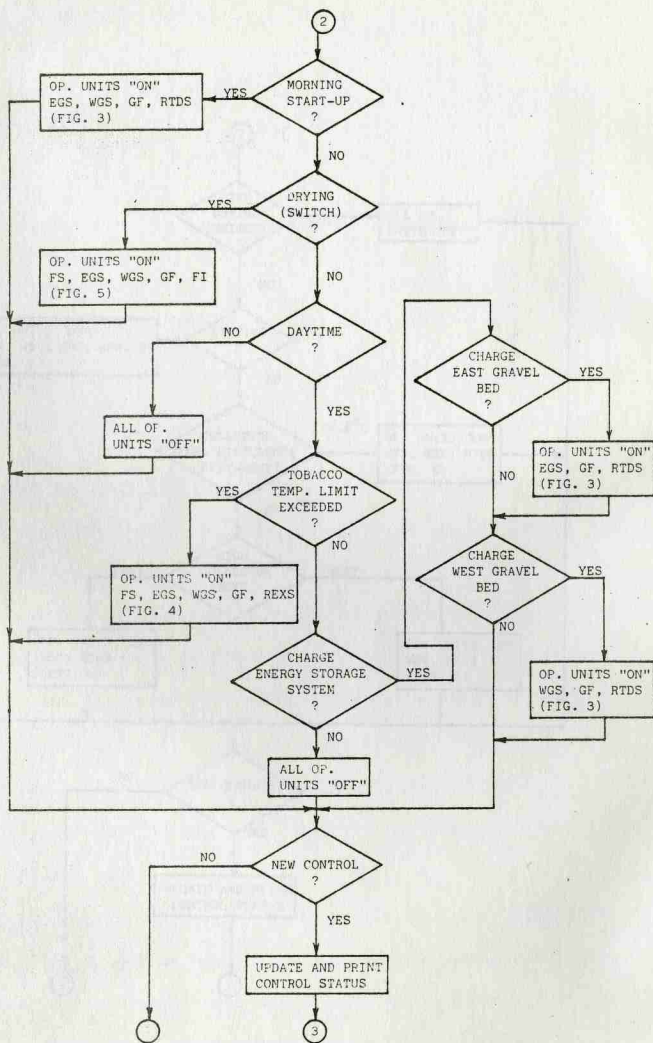


Fig. 9. Yellowing and First Day Leaf Drying.

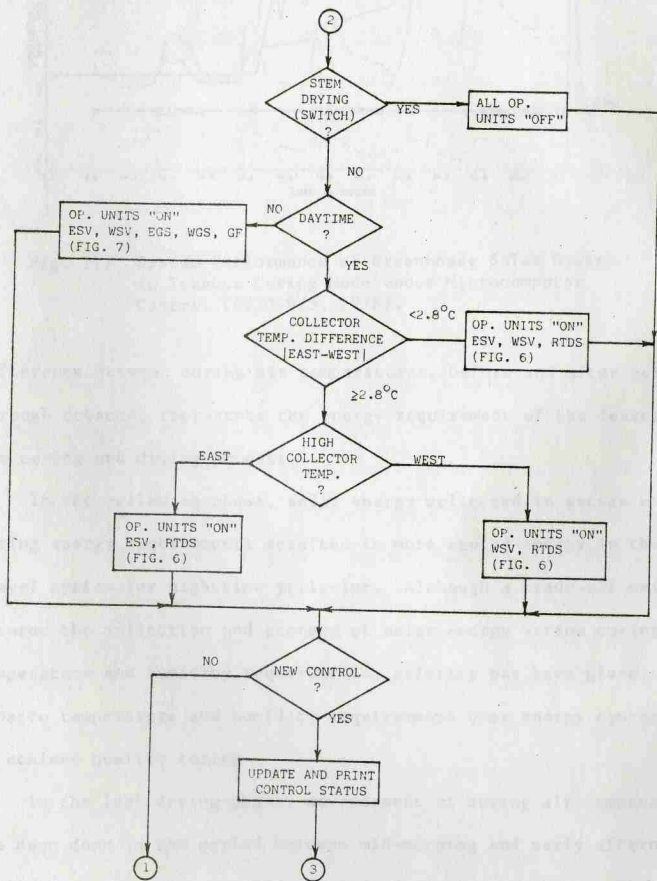


Fig. 10. Leaf and Stem Drying.

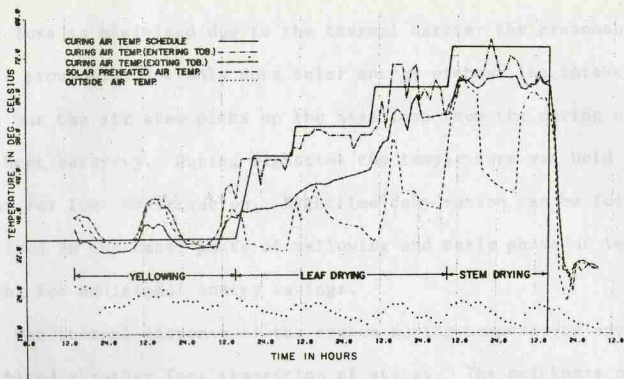


Fig. 11. System Performance of Greenhouse Solar System in Tobacco Curing Mode Under Microcomputer Control (8/30-9/5, 1978).

difference between curing air temperatures, before and after going through tobacco, represents the energy requirement of the leaves during the curing and drying process.

In the yellowing phase, solar energy collected in excess of the curing energy requirements resulted in more stored energy in the gravel system for nighttime yellowing. Although a trade-off exists between the collection and storage of solar energy versus curing temperature and humidity requirements, priority has been given to tobacco temperature and humidity requirements over energy conservation to achieve quality curing.

In the leaf drying phase, advancement of curing air temperature has been done in the period between mid-morning and early afternoon until the temperature reached the stem drying temperature. This is to take full advantage of the inherent design features of the system as a multi-directional, integrated solar collector, to achieve a maximum air preheating. During daytime the solar barn's curing chamber

heat loss is minimized due to the thermal barrier the greenhouse outer-shell provides. Not only does solar energy preheat the intake furnace air, but the air also picks up the heat loss from the curing chamber for heat recovery. During nighttime the temperature was held at the level for fuel conservation. Nighttime dehydration can be fully utilized in the later phase of yellowing and early phase of leaf drying for additional energy savings.

The thermal response of the system during temperature advancement exhibited a rather fast transition of states. The quickness of the system dynamic response illustrates design optimization has been achieved adequately. Full scale tobacco cures with the solar system have demonstrated quality tobacco curing with a 47 to 54 percent fuel savings depending on weather for this system as compared to a conventional bulk curing barn under the same curing management.

Field tests have shown that under favorable weather conditions, the greenhouse solar system provides sufficient solar energy for drying grain or peanuts without using any fossil fuels. For example, approximately 1542 kg of peanuts having a moisture content of 22.9% was dried using solar energy along in Clayton, N.C. (latitude $35^{\circ} 41'N$) on October 24, 1978. The moisture content was reduced to 15.6% within 3 hours in the afternoon as shown in Fig. 12. In this figure the simulated peanut moisture content curve has been calculated based on the moisture gain of drying air passed through peanuts. The drying was discontinued at night. On the second day the moisture content was reduced to about 11.5% with 5 hours of solar drying. Similar results were obtained for rice drying at Kaosiung (latitude $22^{\circ} 42'N$) in mid-December [18].

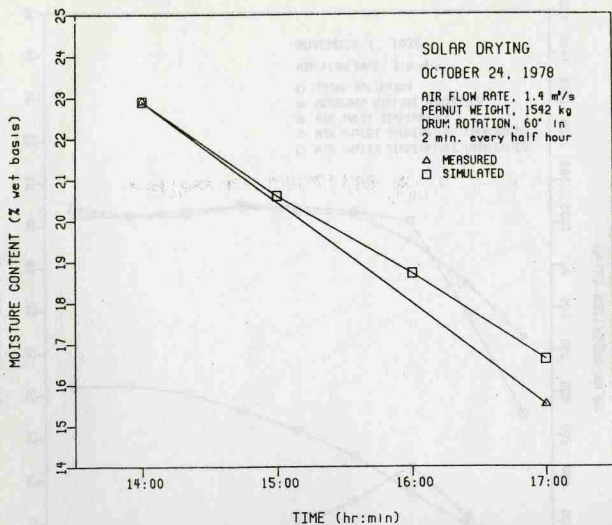


Fig. 12. Solar Curing and Drying of Peanuts Showing Measured and Simulated Drying Rate.

In order to verify the validity of a model for predicting the air temperature inside the greenhouse solar system, a comparison of the measured and simulated air temperature is shown in Fig. 13 for a clear day on November 1, 1978. The simulation result conforms well except for the late afternoon hours. This is because the solar energy stored in the internal elements as sensible heat dissipates into the air inside the structure. As the solar radiation intensity decreases during late afternoon, the effects of transient heat dissipation becomes noticeable.

Based on this analysis, the effects of various system input parameters such as solar radiation intensity, air flow rate through

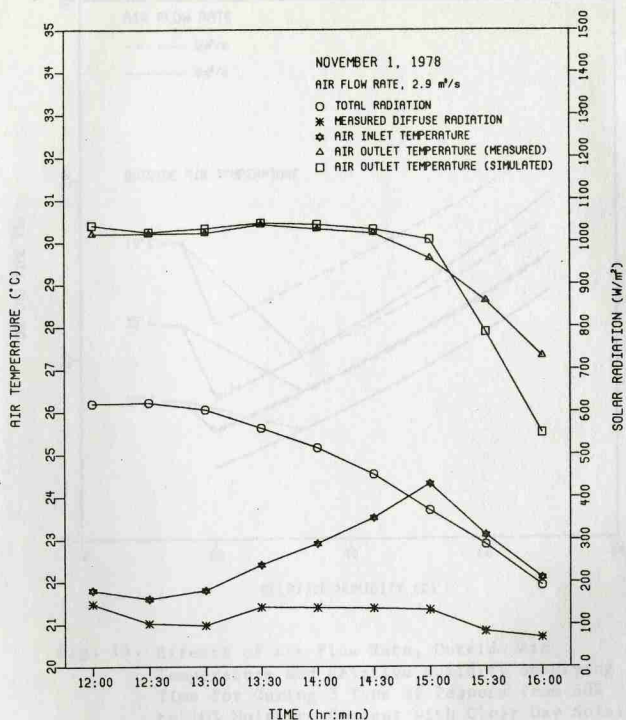


Fig. 13. System Performance of Greenhouse Solar System in Grain Drying Mode Showing Solar Radiation, Inlet Air Temperature, and Measured and Simulated Outlet Air Temperatures.

the system, temperature and humidity of outside air, the effect of solar radiation absorptivity of floor surface on heating of air inside the structure, and drying time were investigated. As a basis for estimating the availability of solar radiation, the ASHRAE [1] solar radiation model for a clear day insolation at a latitude $35^{\circ} 41'N$ was used.

Figure 14 shows the effects of air flow rate, outside air temperature and

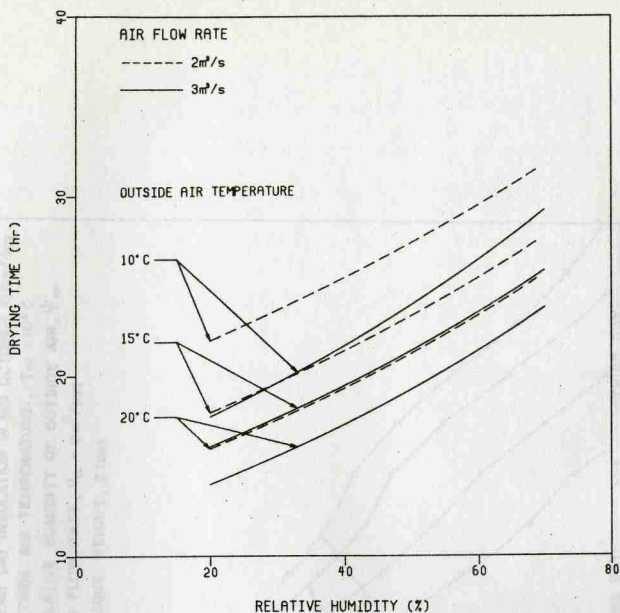


Fig. 14. Effects of Air Flow Rate, Outside Air Temperature and Relative Humidity on Drying Time for Curing 3 Tons of Peanuts from 30% to 10% Moisture Content with Clear Day Solar Insolation in Mid-October.

relative humidity on drying time for curing 3 tons of peanuts, assuming that the peanuts were dried from an initial moisture content of 30% to the final moisture content of 10% with clear day solar insolation in mid-October. The simulated results shown in Fig. 15 indicate that if the continuous solar drying were allowed the moisture content of peanuts could be reduced from 30% to 10% with solar energy alone in 21 to 30 hours. Under practical conditions, weather and nighttime interruption of solar radiation would prolong total drying period beyond 40 hours to provide high quality peanuts.

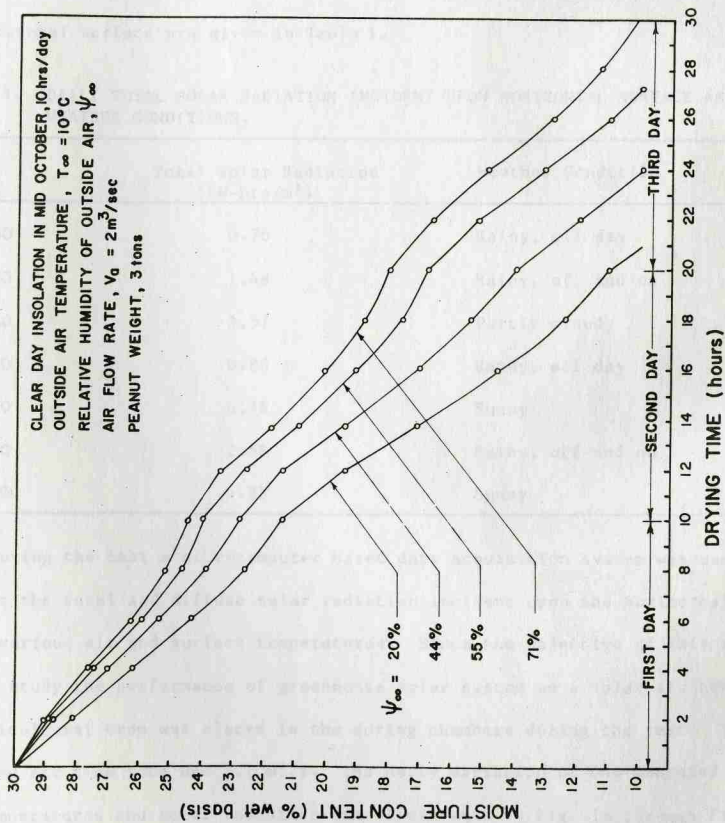


Fig. 15. Simulated System Performance of Greenhouse Solar Drying System with a 6-ton Drum Unit for Solar Peanut Curing.

The performance study of the greenhouse solar system was conducted during the fall of 1980 and the data were taken from September 30 to October 7, 1980. The weather conditions and the total solar radiation incident on a horizontal surface are given in Table 3.

TABLE 3. DAILY TOTAL SOLAR RADIATION INCIDENT UPON HORIZONTAL SURFACE AND WEATHER CONDITIONS.

Date	Total Solar Radiation (kW-hrs/m ²)	Weather Condition
9-30-80	0.76	Rainy, all day
10-1-80	1.48	Rainy, off and on
10-2-80	3.57	Partly cloudy
10-3-80	0.88	Rainy, all day
10-4-80	4.76	Sunny
10-5-80	2.58	Rainy, off and on
10-5-80	4.85	Sunny

During the test a microcomputer based data acquisition system was used to monitor the total and diffuse solar radiation incident upon the horizontal surface, various air and surface temperatures. Since the objective of this study was to study the performance of greenhouse solar system as a solar air heater, no agricultural crop was placed in the curing chambers during the test. The measured air flow rate was 3.1 m³/s. The daily variation of the measured air temperatures and solar radiation are illustrated in Fig. 16 through Fig. 22. The results show that the difference between the inlet and the outlet air temperatures is proportional to the solar radiation intensity and the outlet

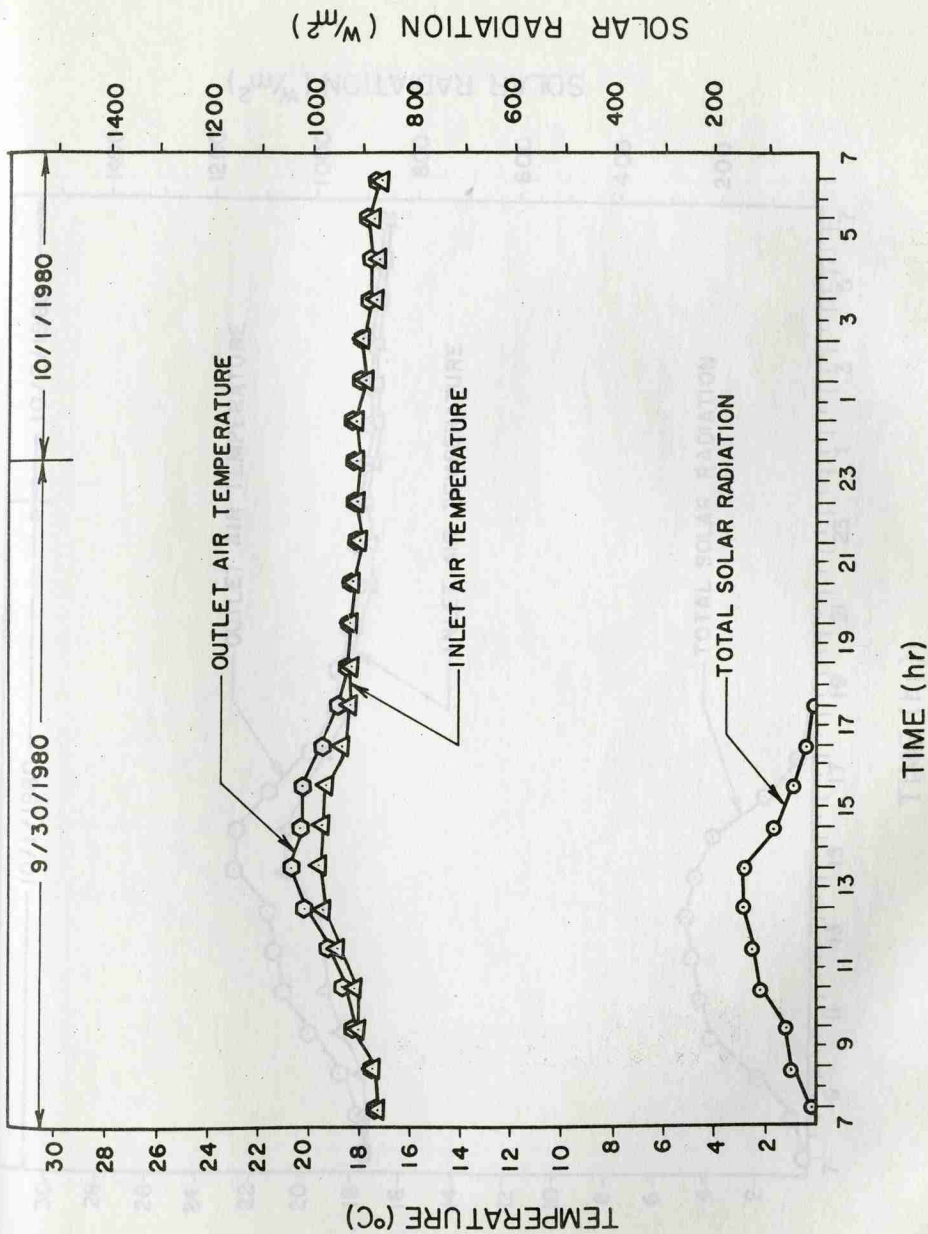


Fig. 16. Total Solar Radiation, Inlet and Outlet Air Temperatures.

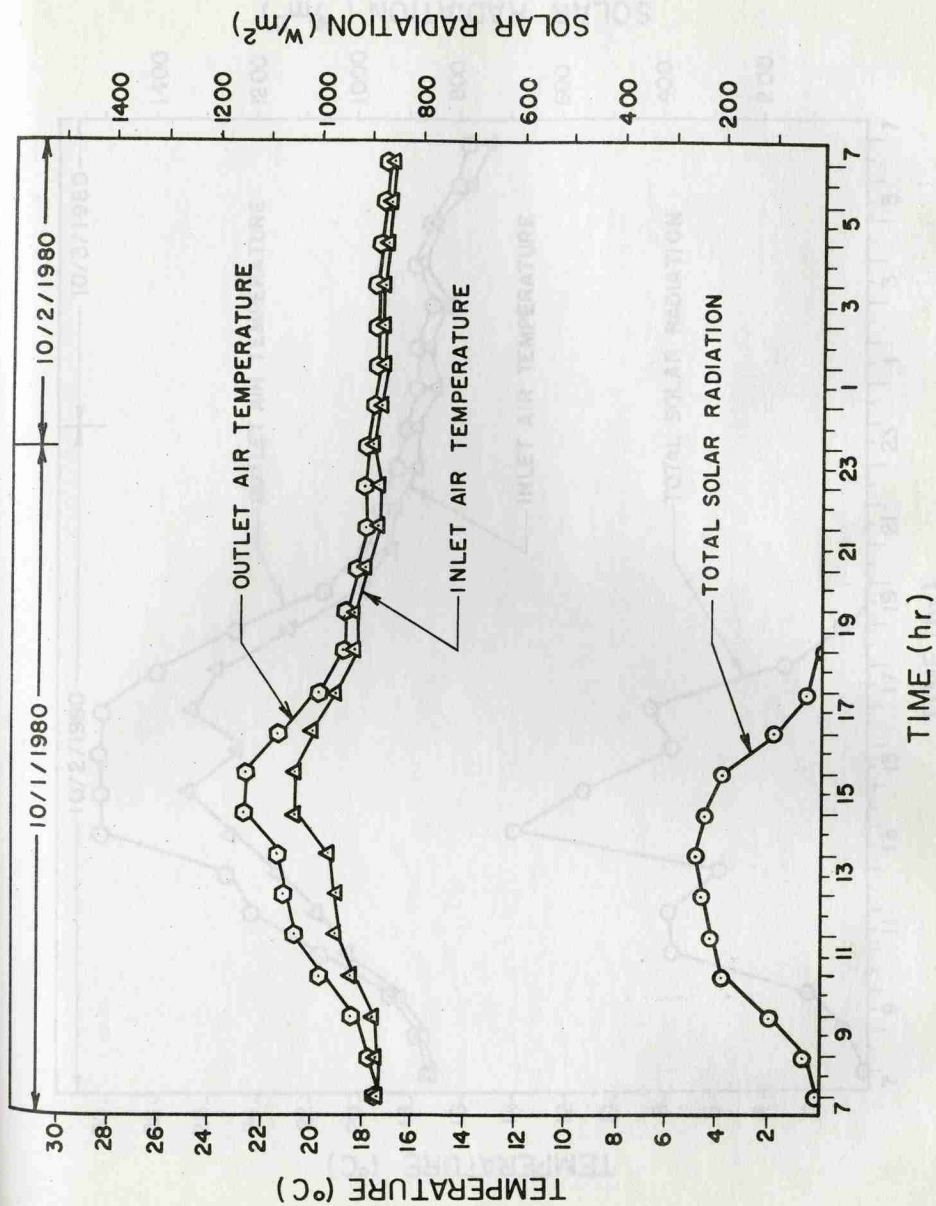


Fig. 17. Total Solar Radiation, Inlet and Outlet Air Temperatures.

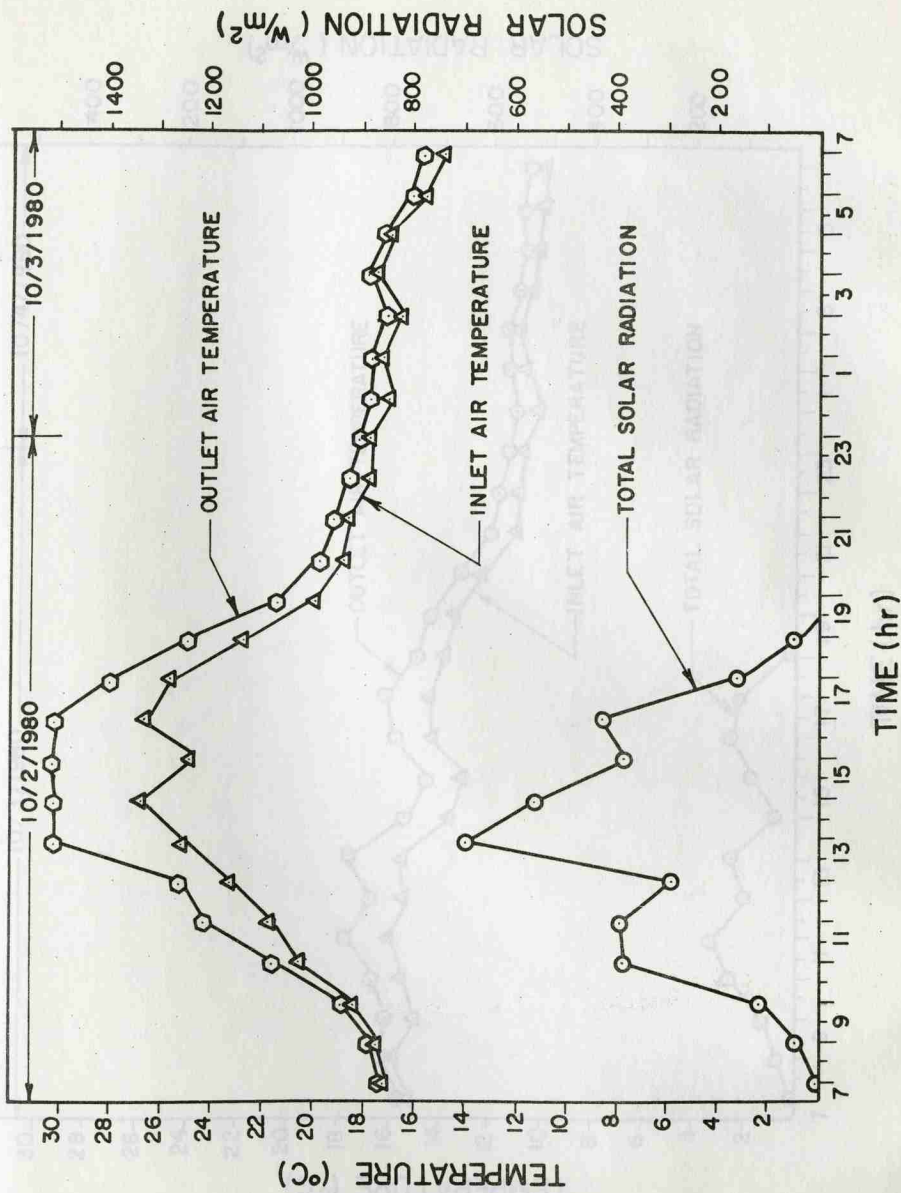


Fig. 18. Total Solar Radiation, Inlet and Outlet Air Temperatures.

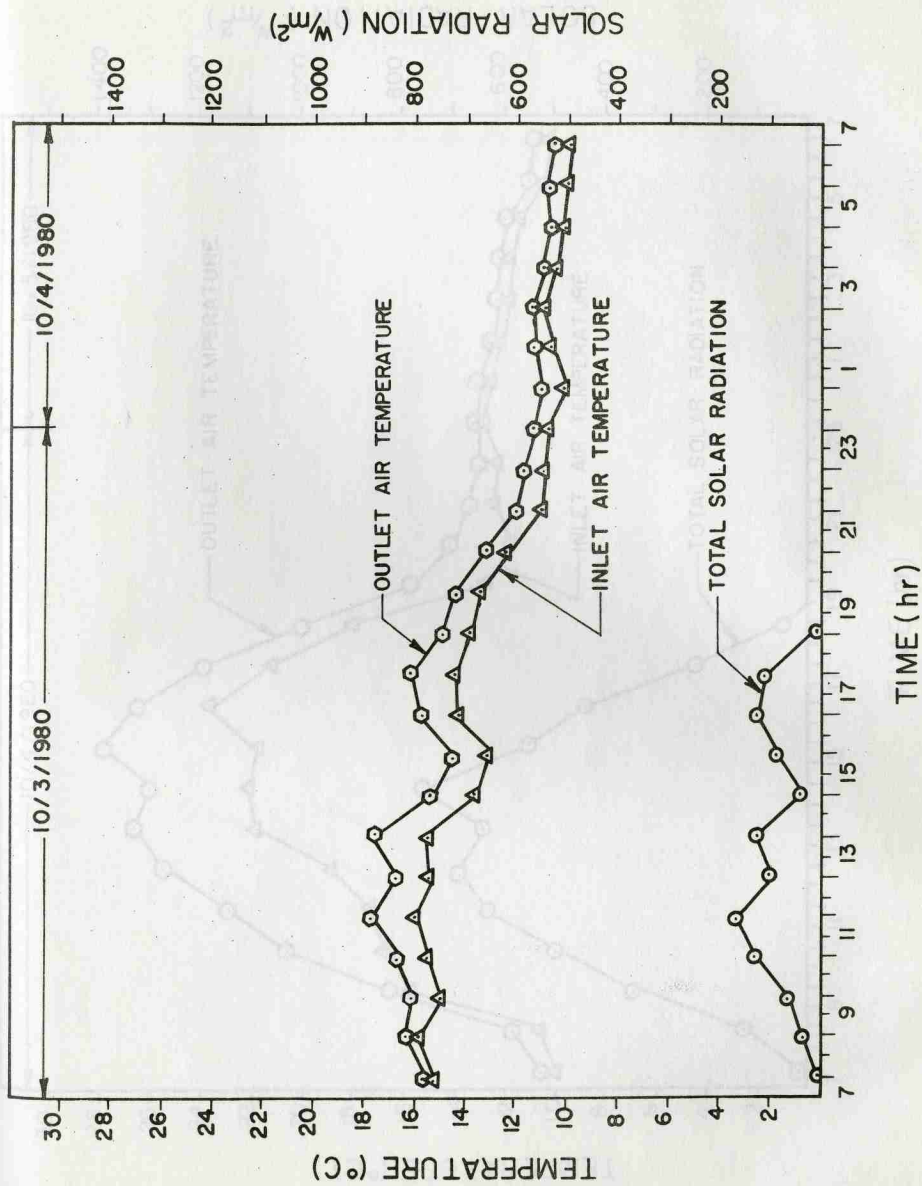


Fig. 19. Total Solar Radiation, Inlet and Outlet Air Temperatures.

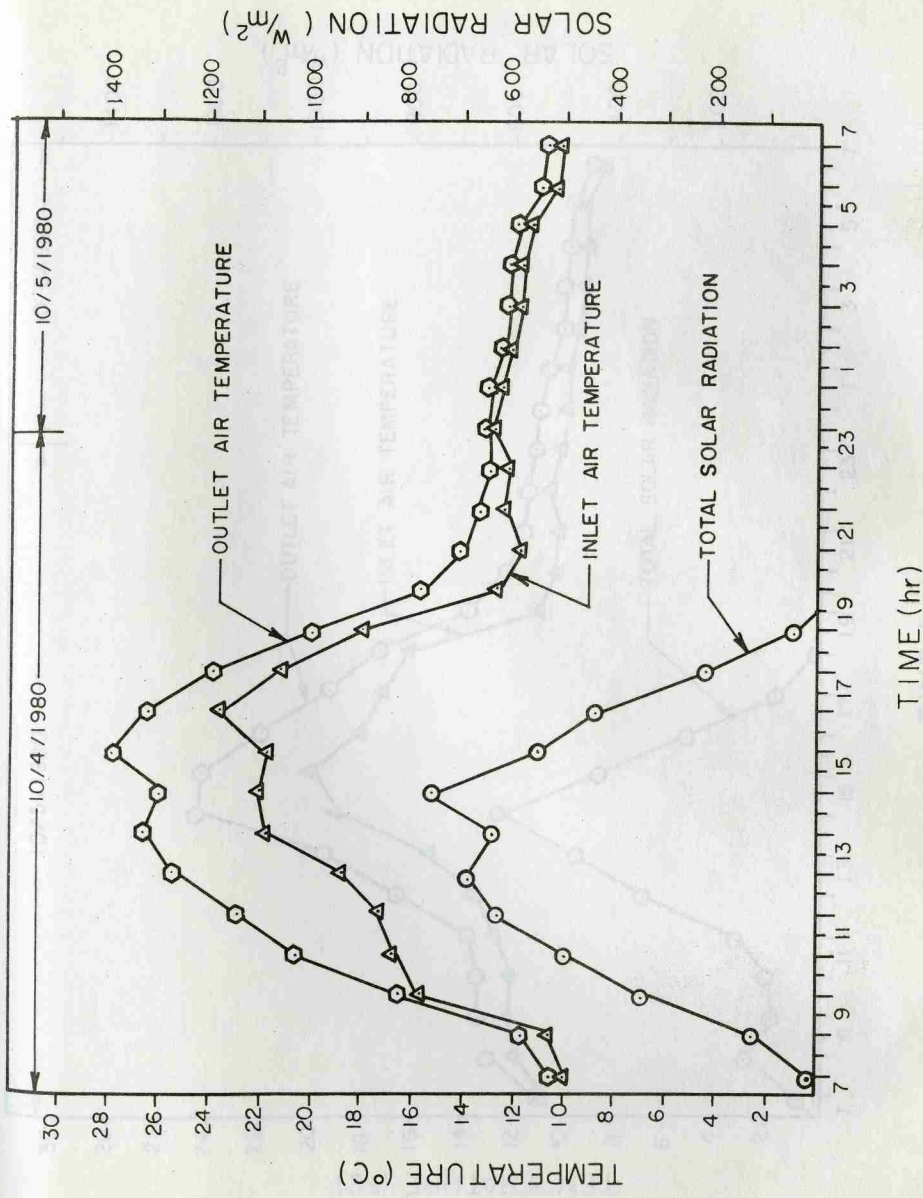


Fig. 20. Total Solar Radiation, Inlet and Outlet Air Temperatures.

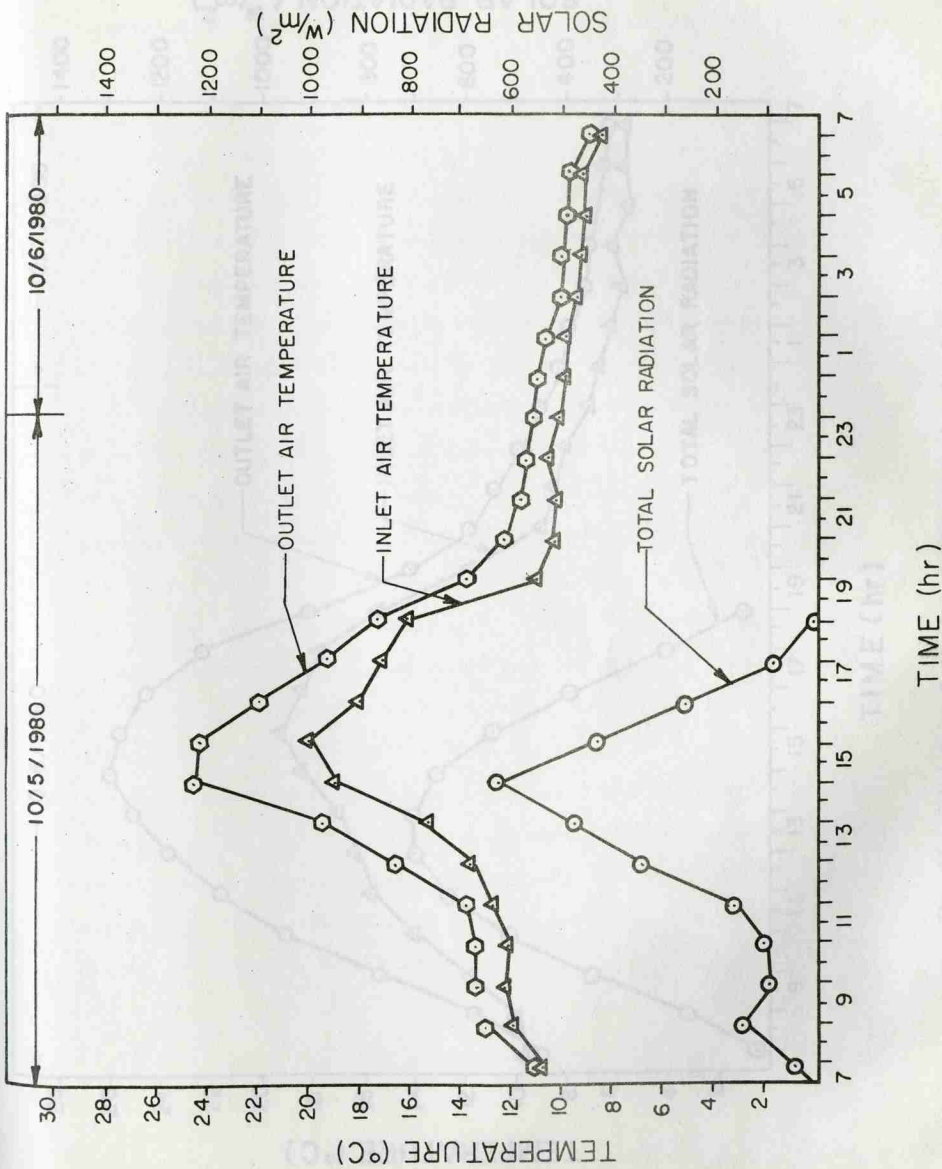
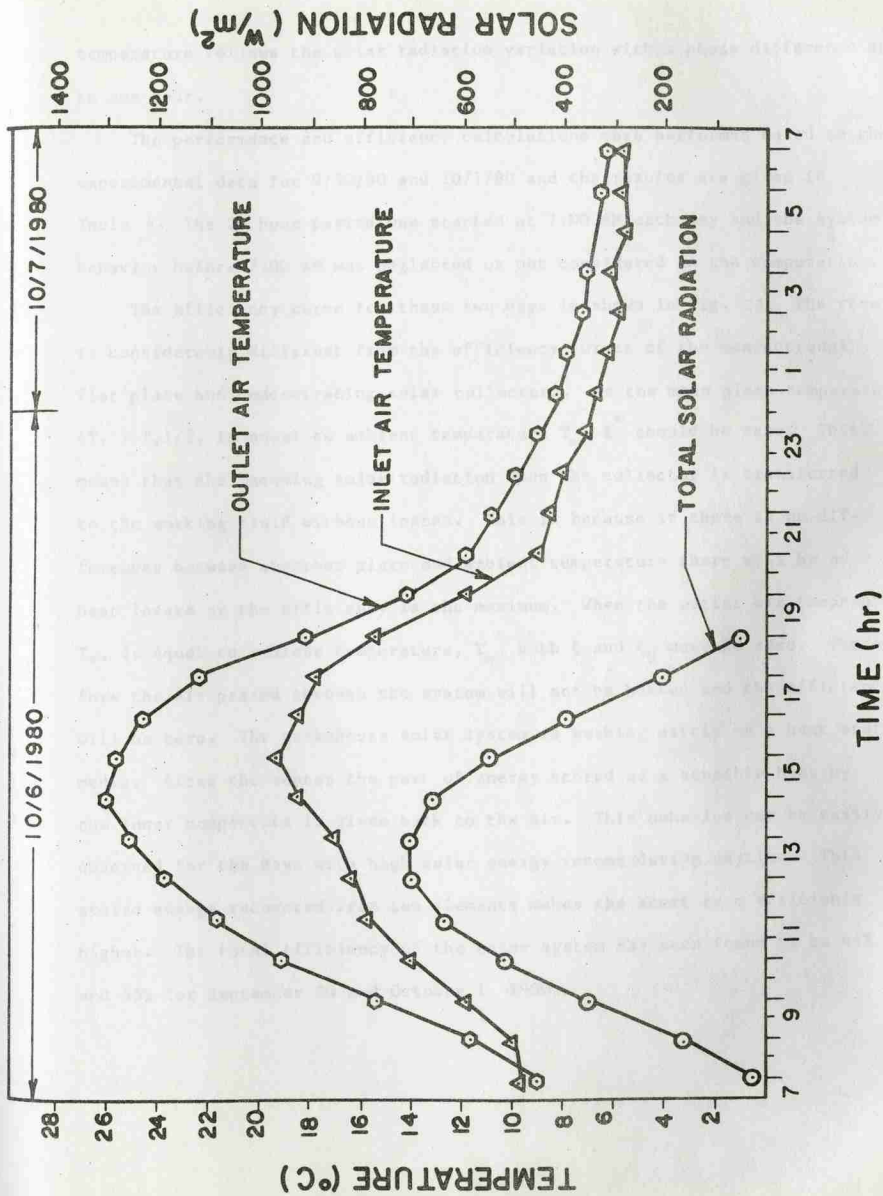


Fig. 21. Total Solar Radiation, Inlet and Outlet Air Temperatures.



temperature follows the solar radiation variation with a phase difference up to one hour.

The performance and efficiency calculations were performed based on the experimental data for 9/30/80 and 10/1/80 and the results are given in Table 4. The 24 hour period was started at 7:00 AM each day and the system behavior before 7:00 AM was neglected or not considered in the computation.

The efficiency curve for these two days is shown in Fig. 23. The result is considerably different from the efficiency curves of the conventional flat plate and concentrating solar collectors. As the mean plate temperature, $(T_1 + T_2)/2$, is equal to ambient temperature T_∞ , ξ^* should be zero. This means that the incoming solar radiation upon the collector is transferred to the working fluid without losses. This is because if there is no differences between absorber plate and ambient temperature there will be no heat losses or the efficiency is the maximum. When the outlet air temperature, T_2 , is equal to ambient temperature, T_∞ , both ξ and ξ_d must be zero. Therefore the air passed through the system will not be heated and the efficiency will be zero. The greenhouse solar system is working partly as a heat storage media. After the sunset the part of energy stored as a sensible heat by the inner components is given back to the air. This behavior can be easily observed for the days with high solar energy income during daytime. This stored energy recovered from the elements makes the short term efficiency higher. The total efficiency of the solar system has been found to be 44% and 55% for September 30 and October 1, 1980.

TABLE 4. TEMPERATURE, SOLAR RADIATION AND SYSTEM EFFICIENCY.

Date	Hours	T_{∞} (°C)	T_2 (°C)	Q_u (KJ/hour)	\bar{I} (W/m ²)	\bar{I}_d (W/m ²)	Q_s (KJ/hour)	η	ξ (°C/W/m ²)
9-30-80	7-8	17.2	17.2	-	-	-	-	-	0.0000
	8-9	17.4	17.4	-	18.30	15.40	6163	-	0.0000
	9-10	18.0	18.1	1605	50.00	40.10	16261	0.09	0.0020
	10-11	18.2	18.5	4814	65.00	52.10	21183	0.22	0.0046
	11-12	18.8	19.2	6419	114.00	90.90	35719	0.17	0.0035
	12-13	19.4	20.2	12838	123.60	101.10	38030	0.33	0.0065
	13-14	19.6	20.7	17652	148.90	121.79	45859	0.38	0.0074
	14-15	19.5	20.4	14443	142.80	118.11	44338	0.32	0.0063
	15-16	19.3	20.3	16048	81.10	67.67	26656	0.60	0.0122
	16-17	18.6	19.5	14443	50.00	41.01	13850	1.04	0.0180
	17-18	18.4	18.9	8024	29.50	29.50	7826	1.02	0.0169
	18-19	18.3	18.5	3209	9.20	9.20	3584	0.89	0.0217
	19-20	18.4	18.4	-	-	-	-	-	-
	20-21	18.3	18.4	1605	-	-	-	-	-
21-22	18.0	18.0	-	-	-	-	-	-	
21-23	18.2	18.2	-	-	-	-	-	-	
23-24	18.1	18.1	-	-	-	-	-	-	
10-1-80	0-1	18.2	18.2	-	-	-	-	-	-
	1-2	17.9	17.9	-	-	-	-	-	-
	2-3	18.0	18.0	-	-	-	-	-	-
	3-4	17.5	17.7	3209	-	-	-	-	-
	4-5	17.4	17.6	3209	-	-	-	-	-
	5-6	17.6	17.7	1605	-	-	-	-	-
	6-7	17.2	17.4	3209	-	-	-	-	-
	7-8	17.3	17.4	1605	4.00	4.00	1180	1.36	0.0250
	8-9	17.4	17.7	4814	35.30	29.80	11730	0.41	0.0085
	9-10	17.6	18.3	11234	92.10	76.70	29449	0.38	0.0076
	10-11	18.4	19.7	20862	195.60	163.60	61130	0.34	0.0066
	11-12	19.0	20.7	27282	212.60	179.40	65670	0.41	0.0080
	12-13	19.1	21.1	32096	232.90	189.10	72551	0.44	0.0086
	13-14	19.4	21.3	30491	248.90	207.90	77649	0.39	0.0760
14-15	20.8	22.7	30491	230.80	194.30	73218	0.42	0.0082	
15-16	20.8	22.6	28886	193.90	167.30	64114	0.45	0.0093	
16-17	20.1	21.4	20862	97.10	81.60	33165	0.59	0.0134	
17-18	19.0	19.8	12838	35.30	33.00	13321	0.96	0.0227	
18-19	18.4	18.9	8024	4.13	4.13	1229	6.53	0.1210	
19-20	18.4	18.7	4814	-	-	-	-	-	
20-21	18.0	18.4	6419	-	-	-	-	-	
21-22	17.6	18.6	6419	-	-	-	-	-	
22-22	17.6	18.1	8024	-	-	-	-	-	
23-24	17.8	18.0	3209	-	-	-	-	-	
10-2-80	0-1	17.5	17.8	4814	-	-	-	-	-
	1-2	17.4	17.6	3209	-	-	-	-	-
	2-3	17.5	17.7	3209	-	-	-	-	-
	3-4	17.5	17.6	1605	-	-	-	-	-
	4-5	17.3	17.5	3209	-	-	-	-	-
	5-6	17.2	17.4	3209	-	-	-	-	-
	6-7	17.1	17.3	3209	-	-	-	-	-

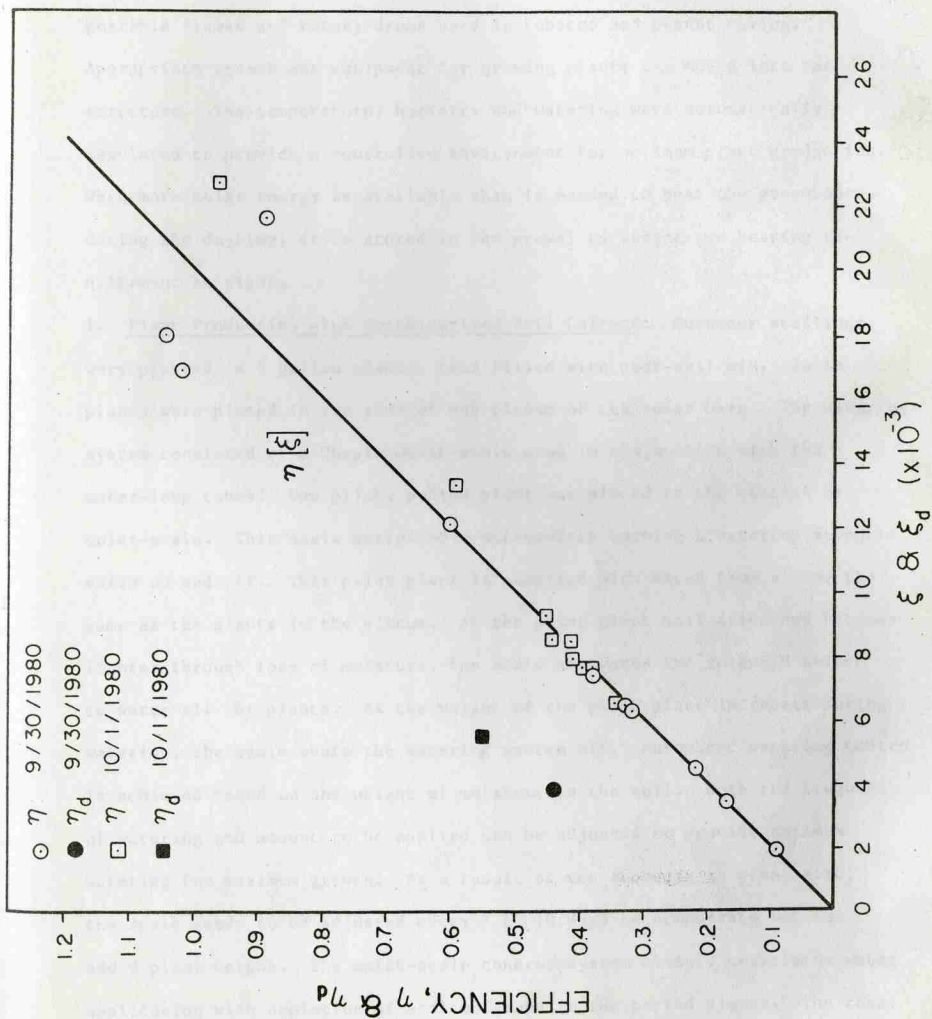


Fig. 23. Efficiency Curve for Bulk-Curing/Greenhouse System.

Greenhouse Mode Operations

At the end of the tobacco and peanut curing seasons the solar barn was converted to greenhouse mode operations by removing the solar absorbers, portable frames and rotary drums used in tobacco and peanut curing. Appropriate greenhouse equipment for growing plants was moved into the structure. The temperature, humidity and watering were automatically regulated to provide a controlled environment for optimum plant production. When more solar energy is available than is needed to heat the greenhouse during the daytime, it is stored in the gravel to reduce the heating requirement at night.

1. Plant Production with Containerized Soil Culture: Cucumber seedlings were planted in 5 gallon plastic pots filled with peat-soil mix. These plants were placed in two rows of one plenum of the solar barn. The watering system consisted of a Chapin moist-scale used in conjunction with the water-loop tubes. One pilot, potted plant was placed on the control or moist-scale. This scale activated a microswitch turning a watering solenoid valve on and off. This pilot plant is supplied with water from a tube the same as the plants in the plenum. As the pilot-plant soil dries and becomes lighter through loss of moisture, the scale activates the solenoid switch to water all the plants. As the weight of the pilot plant increases during watering, the scale shuts the watering system off. Automatic watering control is achieved based on the weight of moisture in the soil. Both the frequency of watering and amount to be applied can be adjusted to provide optimum watering for maximum growth. As a result of the increase in plant size, the scale needs to be adjusted every 7 to 10 days to compensate for the added plant weight. The moist-scale control system closely correlates water application with depletion of soil moisture in the potted plants. The total

weight of cucumbers harvested for 20 plants was 61,821 g, or the average harvest per plant was 3091.05 g. The average fruit size was 192.59 g. Figure 24 shows the cucumber production with containerized soil culture in the solar barn.

2. Plant Production with Hydroponic Culture: To facilitate the conversion of the solar greenhouse bulk curing system from the curing mode to the greenhouse mode, a study was initiated to develop a hydroponic plant production system for the structure. The water culture technique was selected for the following reasons: (1) The three plenums of the structure could be used to contain the nutrient solution for the hydroponic culture, and (2) The nutrient solution could be used for solar energy storage during plant production period. This approach would minimize handling of growth media and containers normally required for greenhouse production.

As shown in Fig. 2(b) solar energy is collected and stored in the greenhouse in two ways. First, solar energy is collected by the greenhouse itself and stored in the two side gravel beds. An auxiliary, reversible gravel fan in the furnace room circulates air within the greenhouse and gravel beds for energy storage and temperature control. In the second way, the nutrient solution in the plenums acts as a heat sink, collecting its energy from the solar panels mounted on the furnace room and from the internal surroundings of the greenhouse. A reversal of this process occurs during the nighttime. The nutrient solution discharges its stored energy to the panels and the surroundings. The 11 solar energy panels mounted on the furnace room are each 1.2336 m wide by 2.4672 m long with flow passages distributed longitudinally. The total panel area represents about 70 percent of the plenum area which is within the recommended area for solar heating of swimming pools.



Fig. 24. Cucumber Production with Containerized Soil Culture in Solar Barn.



Fig. 25. Tomato Production with Hydroponic Culture in Solar Barn.

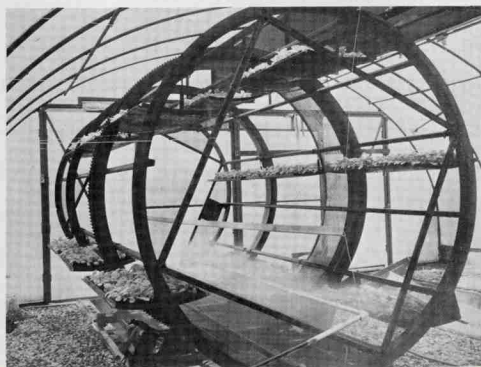
Tomato production (Fig. 25) averaged 8.6 lbs/plant for the 19 week period the plants were grown. This production average only represented a fraction of the total production possible since tomato plants produce for 8 to 9 months before production declines. The largest tomato produced weighed 1.57 lbs.

3. Tobacco Transplant Production: Tobacco transplants were grown in seedling growing and handling trays [31] in the solar barn for automatic transplanting and for conducting three-year comparison studies in growth and yield of transplants produced in the solar barn versus the conventional plantbed. Tobacco transplants were grown using two approaches for maximum space utilization. As shown in Figs. 2(a) and 26, one method uses four stationary layers utilizing the portable frames used for tobacco curing. The second approach uses a rotary layer system utilizing rotary drums used for grain or peanut drying for more uniform watering and lighting.

The stationary layers consist of perforated sheet metal covered supports spaced approximately 63.5 cm apart in the portable frames. An automated misting system is used on each layer using propagation nozzles at 100 psi to provide fine misting for approximately 15 seconds per 30 minutes during daylight hours. High germination rates of 95-97 percent were obtained on each layer 7 to 8 days after seeding. Uniform growth in early stages of transplant growth were achieved in all three layers of seedling production. Variations in light levels and misting both within and between layers contributed to visible non-uniform growth after 3-4 weeks. To correct this environmental growth problem seedlings were mowed to trim larger leaves. This action tended to normalize the plant canopy and keeps plants at approximately the same size. The perforated surface of the rotary drum was designed to be disassembled to serve as hanging trays of a ferris wheel plant production



(a)



(b)

Fig. 26. Automated Tobacco Seedling Production Systems: (a) Stationary Layer System Utilizing Portable Frames; (b) Rotary Layer System Utilizing Rotary Drums.

system as shown in Fig. 26(b). The rotating device for the drum was utilized to provide periodic rotation. An automated watering system provided misting at the bottom of the drum during its rotation. Temperatures in the solar barn were maintained between 22°C minimum and 29°C maximum during the day and 18°C minimum at night. Thermostats controlled a solar barn LP gas heater and two vent fans to maintain these temperatures. A chemical solution feeder automatically provided nutrient as the tobacco transplants were misted.

Figure 27 shows the tray, tobacco transplants being pulled from the tray cells, and the effect of air pruning on plant roots. Air pruning maintains uniform root and shoot system for an approximately constant shoot-root ratio of a plant. The trays were designed to adapt to the transplanter indexing frame which holds six trays or 480 plants. A commercial version of the two-row automatic transplanter made by the Harrington Manufacturing Company (Fig. 28) was field tested using the tobacco transplants grown in the solar barn.

The curves shown in Fig. 29 indicate that the air pruned tobacco plants transplanted from the greenhouse were growing considerably better than those from the conventional plantbed. Even with their smaller initial sizes, the air-pruned intact root transplants exceeded the conventionally grown transplants and resulted in significantly higher yield. The curves also show that the differences in transplant sizes became less as the plants grew in the field. The statistical analysis of the yield data shows no significant difference in yield for transplant size, but shows a significant difference in yield for transplant source at the 5 percent level [21].

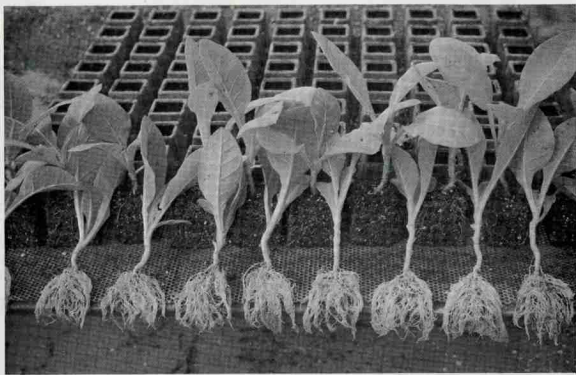


Fig. 27. Seedling Growing and Handling Tray, Tobacco Transplants Pulled out from the Tray Showing the Effect of Air Pruning on Plant Roots to Maintain Uniform Root System.



Fig. 28. Field Transplanting of Solar Barn Grown Tobacco Transplants Using the Two-Row Fully Automatic Transplanter.

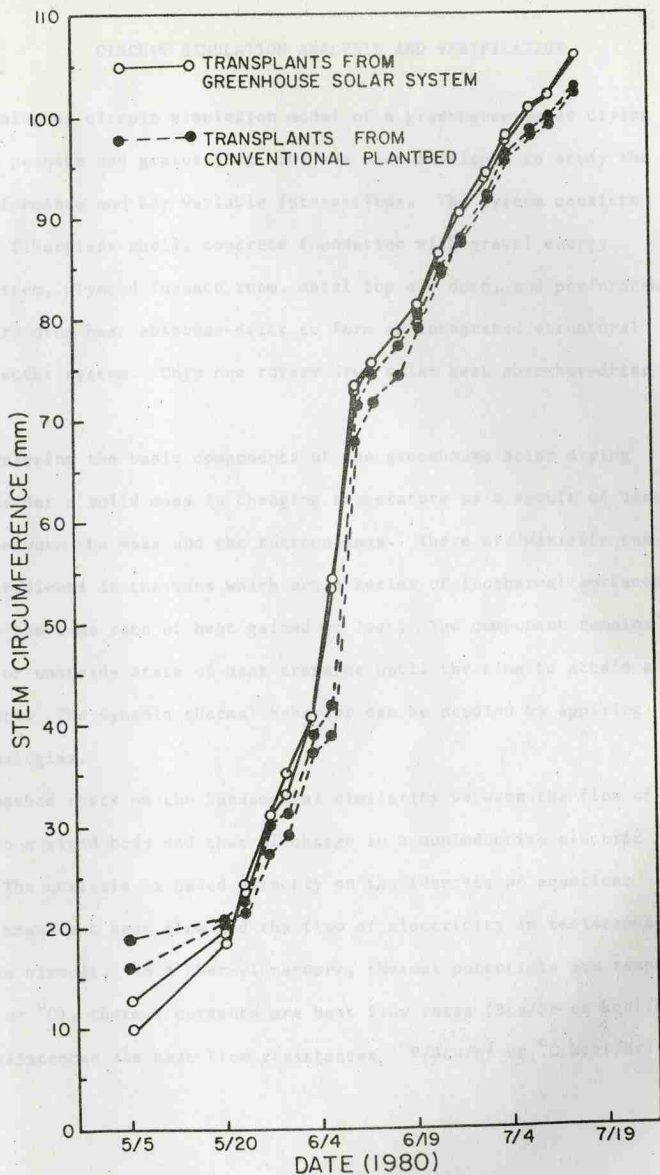


Fig. 29. Growth Curves for Tobacco Plants Transplanted from Greenhouse Solar System and Conventional Plantbed.

CIRCUIT SIMULATION ANALYSIS AND VERIFICATION

An analogous circuit simulation model of a greenhouse solar drying system for peanuts and grains (Fig. 30) has been developed to study the system performance and key variable interactions. The system consists of a clear fiberglass shell, concrete foundation with gravel energy storage system, plywood furnace room, metal top air duct, and perforated metal rotary drum heat absorber-drier to form an integrated structural solar collector system. Only one rotary drum solar heat absorber-drier was used.

In analyzing the basic components of the greenhouse solar drying system consider a solid mass is changing temperature as a result of heat exchange between the mass and the surroundings. There are variable temperature gradients in the mass which are a series of isothermal surfaces related to the time rate of heat gained or lost. The component remains in transient or unsteady state of heat transfer until the time to attain a steady state. The dynamic thermal behavior can be studied by applying dynamic analogies.

The method rests on the fundamental similarity between the flow of heat within a rigid body and that of charge in a noninductive electric circuit. The analysis is based directly on the identity of equations governing transient heat flow and the flow of electricity in resistance-capacitance circuit. In a thermal network, thermal potentials are temperatures ($^{\circ}\text{F}$ or $^{\circ}\text{C}$), thermal currents are heat flow rates (Btu/hr or kcal/hr), thermal resistances are heat flow resistances ($^{\circ}\text{F}/\text{Btu/hr}$ or $^{\circ}\text{C}/\text{kcal/hr}$),

thermal capacitances are heat storage elements (Btu/^oF or kcal/^oC), and thermal sources or sinks respectively produce heat or receive heat (Btu/hr or kcal/hr).

In general, analyzing a system by the thermal circuit method requires:

- (1) complete description of the physical system with a sketch including dimensions, thermal properties, system input in temperature and/or heat flow rate, and independent variables in the surroundings of the system;
- (2) drawing of thermal circuit; (3) calculation of resistances and capacitances; (4) writing of circuit equations; (5) solving of circuit equations; and (6) interpretation of results. Utilization of an electronic circuit analysis program with digital computer would reduce steps (4) and (5) into simple programming and computer run including computer plotting.

In drawing the thermal circuit for the greenhouse solar drying system, the system components are idealized and represented by circuit elements as shown in Fig. 30. The symbols for the circuit elements are described in Table 5. The thermal properties of materials used are given in Table 6.

TABLE 5. NOMENCLATURE AND SYMBOLS.

Symbols	Subscripts
R = conduction resistance	f ₁ = tilted fiberglass wall
R _{co} = outside convection resistance	f ₂ = vertical fiberglass wall
R _{ci} = inside convection resistance	h = heat absorber
R _{ri} = inside 'surface' radiation resistance	d = top air duct
R _{xy} = inside 'space' radiation resistance	g = gravel energy storage
C = capacitor	p = plywood wall
T _i = inside air temperature	a = air space
T _o = outside air temperature	e = electrical circuit element
Q _s = solar radiation input	t = thermal circuit element
R _e = equivalent resistance (~5000 x 10 ³ ohms)	
θ = time	

TABLE 6. THERMAL PROPERTIES OF MATERIALS USED.

Material	Thermal Conductivity	Heat Capacity	Mass Density
	K Btu/(hr)(ft)(°F)	C _p Btu/(lb)(°F)	γ lb/(cu ft)
Douglas Fir Wood (½")	0.065	0.5	34*
Fiberglass (0.04")	0.02	0.2	~90 ^Δ
Iron Plate (1/16")	31.00	0.11	490 ⁺
Gravel	0.42	0.22	120 ⁺
Air	0.016	0.24	0.072*

* Holman, J.P. 1972. Heat Transfer. McGraw-Hill Book Co.

^Δ Knox, R.E. 1963. Insulation properties of fluorcarbon expanded rigid urethane foam. Trans. ASHRAE, Vol. 69, p. 150.

⁺ Kent, R.T. 1946. Kent's Mechanical Engineers' Handbook, 11th Ed. John Wiley

Analogous variables of different physical systems can be interrelated quantitatively. Interconversion of corresponding thermal and electrical quantities can be obtained by defining the scale factor as;

$$\text{Scale Factor} = \frac{\text{Magnitude of quantity unit in electrical circuit}}{\text{Magnitude of quantity unit in thermal circuit}} \quad (65)$$

The units and scale factors of analogous electrical and thermal parameters are shown in Table 7.

TABLE 7. UNITS AND SCALE FACTORS OF ANALOGOUS ELECTRICAL AND THERMAL PARAMETERS.

Quantity	Units			Scale Factors		
	Electrical	Thermal		Ratio	Value	
		British	SI		British	SI
Time	sec	hr	hr	$\frac{\theta_e}{\theta_t}$	2	2
Capacity	farad	$\frac{\text{Btu}}{^\circ\text{F}}$	$\frac{\text{kcal}}{^\circ\text{C}}$	$\frac{C_e}{C_t}$	$\frac{1}{8 \times 10^6}$	$\frac{1}{4 \times 10^6}$
Resistance	ohm	$\frac{^\circ\text{F}}{(\text{Btu/hr})}$	$\frac{^\circ\text{C}}{(\text{kcal/hr})}$	$\frac{R_e}{R_t}$	16×10^6	8×10^6
Potential	volt	$^\circ\text{F}$	$^\circ\text{C}$	$\frac{E}{T}$	1	1
Rate of Energy Transfer	$\frac{\text{coulomb}}{\text{sec}}$ or ampere	$\frac{\text{Btu}}{\text{hr}}$	$\frac{\text{kcal}}{\text{hr}}$	$\frac{I}{Q}$	$\frac{1}{16 \times 10^6}$	$\frac{1}{8 \times 10^6}$

The calculation procedures in the analysis can be summarized and illustrated by the following successive steps:

A thermal conduction resistance is calculated from the following equation;

$$R_t = \frac{L}{KA} \left(\frac{^{\circ}\text{F}}{\text{Btu/hr}} \right) \quad (66)$$

where

L = length of the conductor, ft

K = thermal conductivity (Btu/hr-ft- $^{\circ}\text{F}$)

A = cross-sectional area, (ft²)

For the vertical fiberglass wall

$$L = \frac{0.04}{12} \text{ ft}, A_{f_2} = 225 \text{ ft}^2, K = 0.02 \left(\frac{\text{Btu}}{\text{hr-ft-}^{\circ}\text{F}} \right)$$

$$(R_{f_2})_t = \frac{\frac{0.04}{12}}{0.02 \times 225} = 0.74 \times 10^{-3} \left(\frac{^{\circ}\text{F}}{\text{Btu/hr}} \right)$$

From Table 6 the value of resistance scale factor is 16×10^6

$$(R_{f_2})_e = 0.74 \times 10^{-3} \times 16 \times 10^6 = 1.185 \times 10^4 \text{ (ohms)}$$

A thermal capacitance is calculated as follows,

$$C_t = c_p \gamma V \text{ (Btu/}^{\circ}\text{F)} \quad (67)$$

where

c_p = unit heat capacity (Btu/lb $^{\circ}\text{F}$)

γ = density (lb/ft³)

V = volume of the mass (ft³)

for the vertical fiberglass wall

$$(C_{f_2})_t = 0.2 \times 90 \times 225 \times \frac{0.04}{12} = 13.5 \text{ (Btu/}^{\circ}\text{F)}$$

$$(C_{f_2})_e = \frac{13.5}{8 \times 10^6} = 1.6875 \times 10^{-6} \text{ (farads)}$$

A convection resistance for a particular surface is by definition $\frac{1}{h_c A}$ in which h_c is the convection coefficient.

The thermal convection coefficient between the exposed surfaces and the outside air, h_{co} , is influenced by the air velocity over the surface. For a wind velocity of 7.5 mph on November 11, 1978, the outside convection coefficient is

$$h_{co} = 4(\text{Btu/hr-ft}^2\text{-}^\circ\text{F})$$

For vertical fiberglass the outside convection resistance can be calculated as

$$(R_{co})_t = \frac{1}{4 \times 225} = 0.11 \times 10^{-2} \left(\frac{^\circ\text{F}}{\text{Btu/hr}} \right)$$

$$(R_{co})_e = 0.11 \times 10^{-2} \times 16 \times 10^6 = 1.78 \times 10^4 \text{ (ohms)}$$

The inside resistance can be estimated based on free convection considering there was no air movement inside the greenhouse (November 11, 1978).

The convection coefficient h_{ci} was estimated as

$$h_{ci} = 1.65 (\text{Btu/hr-ft}^2\text{-}^\circ\text{F})$$

$$(R_{ci})_t = \frac{1}{0.325 \times 225} = 0.269 \times 10^{-2} \left(\frac{^\circ\text{F}}{\text{Btu/hr}} \right)$$

$$(R_{co})_e = 0.269 \times 10^{-2} \times 16 \times 10^6 = 4.31 \times 10^4 \text{ (ohms)}$$

Radiation exchange network accounting for direct radiation between surfaces within the solar collector was calculated based on the following equations (68) and (69). The shape factors, F_{in} , required to evaluate

the network resistors were computed with the aid of equations and charts.

The values of surface emissivity, ϵ , used in the calculation are 0.95 for

heat absorber, air duct, and plywood and 0.7 for gravel. An average surface temperature, T_{av} , of 526 Rankin and the Stefan-Boltzmann constant, σ , of 0.1713×10^{-9} Btu/hr-ft²-°R⁴ are used in the evaluation of resistance.

$$(R_{ri})_t = \frac{1 - \epsilon}{4 A_{f_2} \epsilon \sigma T_{av}^3} \quad (68)$$

$$= \frac{0.05}{4 \times 225 \times 0.95 \times 0.1713 \times 10^{-9} \times (526)^3} = 2.34 \times 10^{-4} \left(\frac{^\circ R}{\text{Btu/hr}} \right)$$

$$(R_{ri})_e = 2.34 \times 10^{-4} \times 16 \times 10^6 = 3.74 \times 10^3 \text{ (ohms)}$$

$$(R_{f,h})_t = \frac{1}{4 A_{hF} \sigma T_{av}^3} \quad (69)$$

$$= \frac{1}{4 \times 1120 \times 0.31 \times 0.1713 \times 10^{-9} \times (526)^3} = 2.89 \times 10^{-3} \left(\frac{^\circ R}{\text{Btu/hr}} \right)$$

$$(R_{f,h})_e = 2.89 \times 10^{-3} \times 16 \times 10^6 = 4.62 \times 10^4 \text{ (ohms)}$$

The solar heat input absorbed by various surfaces of the solar collector can be evaluated with the following equations [28].

$$Q_s = (q)(\text{coeff. of transparency of the fiberglass, } 0.75) \times (\text{absorptivity of the surface})(\text{area of the surface}) \quad (70)$$

$$q = \frac{\cos \theta}{\sin \beta} (H_t - H_d) + \frac{1}{2} (1 + \cos \phi) H_d \quad (71)$$

$$\cos \theta = \cos \beta \cos \psi \sin \phi + \sin \beta \cos \phi \quad (72)$$

$$\sin \beta = \cos L \cos H \cos D + \sin L \sin D \quad (73)$$

q = total radiation incident upon tilted surface per unit time per unit area (Btu/hr-ft²)

H_t = total radiation incident upon a horizontal surface per unit time per unit area (Btu/hr-ft²)

H_d = diffuse radiation incident upon a horizontal surface per unit time per unit area (Btu/hr-ft²)

θ = incident angle of solar energy upon tilted surface

β = altitude angle of the sun

ϕ = tilted angle of the surface from the horizontal

ψ = wall solar azimuth angle

L = latitude

H = hour angle

D = sun's declination

The calculation of Q_d for air duct as a heat source was performed using the above equations and $A_d = 112 \text{ ft}^2$, $H = 60^\circ$, $L = 36^\circ$, $\psi = 0$, $\phi = 90^\circ$, $D = 23\frac{1}{2}$.

$$\sin\theta = 0.81 \times 0.92 \times 0.5 + 0.588 \times 0.399 = 0.6075$$

$$\cos\theta = 0.794$$

$$q = \frac{0.794}{0.6075} (7.09 - 7.1) + (\frac{1}{2} \times 7.1) = 3.536$$

$$Q_d = 3.536 \times 0.75 \times 0.95 \times 112 = 2.8265 \times 10^2$$

$$I = \frac{2.8265 \times 10^2}{16 \times 10^6} = 1.766 \times 10^{-5}$$

The air capacitance was calculated for no air movement inside the greenhouse shell,

$$(C_a)_t = c_p \gamma V$$

$$= 0.24 \times 0.072 \times 6.0648 \times 10^3 = 1.048 \times 10^2 \left(\frac{\text{Btu}}{^\circ\text{F}}\right)$$

$$(C_a)_e = \frac{1.048 \times 10^2}{8 \times 10^6} = 1.31 \times 10^{-5} \text{ (farads)}$$

The drum surface temperatures were evaluated based on heat flow equation

$$Q_h = c_p V \Delta T \quad (74)$$

in which

$$V = 21.875 \text{ ft}^3, \gamma = 490 \text{ lb/ft}^3, c_p = 0.11 \text{ Btu/lb}^\circ\text{F}, Q_h = 4832.688 \frac{\text{Btu}}{\text{hr}}$$

and $T_a = 59.1^\circ\text{F}$ at 8:00.

$$\Delta T = \frac{4832.688}{21,875 \times 490 \times 0.11} = 4.1^{\circ}\text{F}$$

$$T_h = 59.1 - 4.1 = 55^{\circ}\text{F}$$

Thermal Circuit Representing Greenhouse Solar Drying System

In working out a proper thermal circuit for the greenhouse solar drying system, it is assumed that the net long-wave radiation exchange between the outer surface of the fiberglass wall and the surroundings is small and can be included in its convection heat transfer. Thermal-energy transfer through all structural elements is considered to be unidirectional and perpendicular to the long dimension. Each of the distributed property section is replaced by lumped property section and all lumped thermal properties are considered to be constant over the temperature range encountered. The air mass in the enclosed space is considered to be at a uniform temperature at any instant.

The circuit elements described in Fig. 30 are combined to form a system thermal circuit shown in Fig. 31. The circuit is basically consisting of three parts:

- (1) Parallel lumped R-C networks representing thermal conduction paths through the structural elements.
- (2) A resistance network representing radiation exchange between all interior surfaces.
- (3) Temperature sources connected through appropriate thermal resistance to the network and heat source at various points in the network representing boundary conditions.

The calculation of the conduction path resistances and capacitances for solar collector components are summarized in Table 8. The summarized results for convection and radiation resistances are respectively shown in Tables 9 and 10.

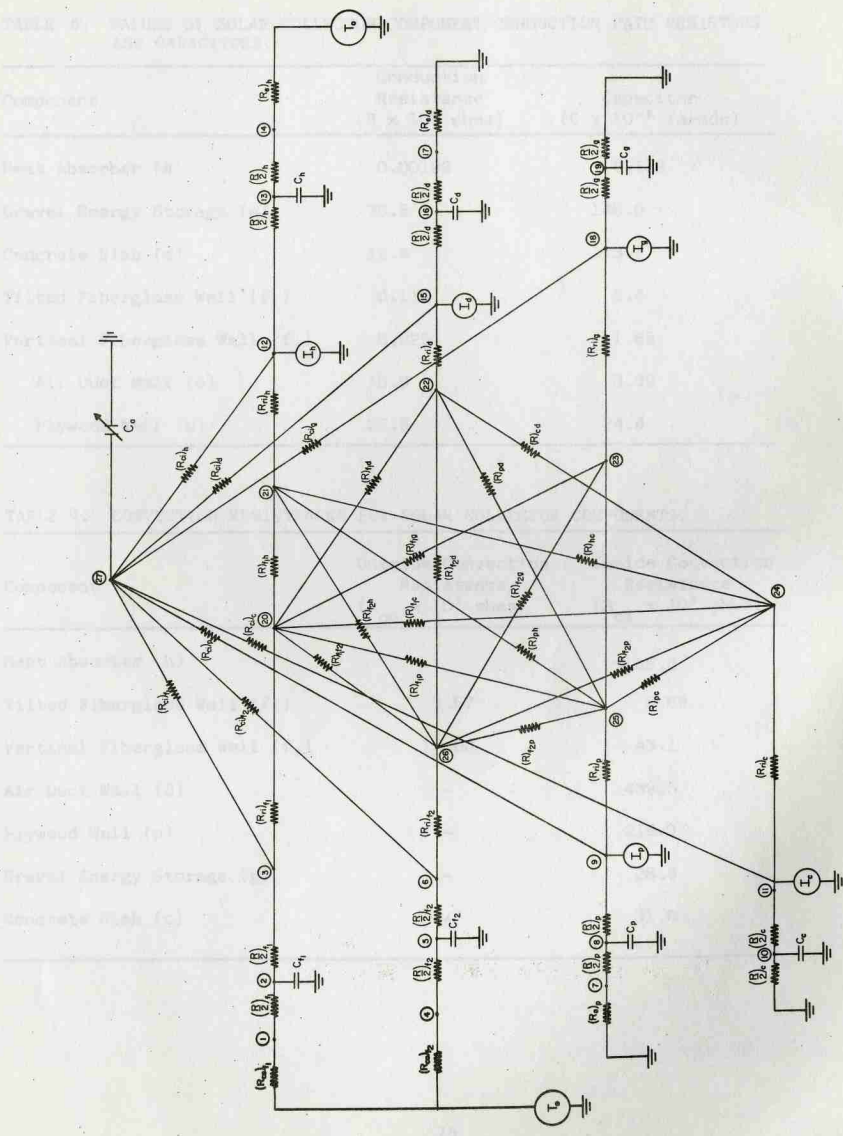


Fig. 31. Thermal Circuit Simulation Model for Greenhouse Solar Drying System.

TABLE 8. VALUES OF SOLAR COLLECTOR COMPONENT CONDUCTION PATH RESISTORS AND CAPACITORS.

Component	Conduction Resistance ($R \times 10^3$ ohms)	Capacitor ($C \times 10^{-6}$ farads)
Heat Absorber (h)	0.00192	6.132
Gravel Energy Storage (g)	75.6	148.0
Concrete Slab (c)	12.4	113.7
Tilted Fiberglass Wall (f_1)	0.119	8.4
Vertical Fiberglass Wall (f_2)	5.925	1.69
Air Duct Wall (d)	10.9	3.39
Plywood Wall (p)	22.8	24.4

TABLE 9. CONVECTION RESISTANCES FOR SOLAR COLLECTOR COMPONENTS.

Component	Outside Convection Resistance ($R_{co} \times 10^3$ ohms)	Inside Convection Resistance ($R_{ci} \times 10^3$ ohms)
Heat Absorber (h)	-	148.0
Tilted Fiberglass Wall (f_1)	3.57	8.66
Vertical Fiberglass Wall (f_2)	17.80	43.1
Air Duct Wall (d)	-	439.5
Plywood Wall (p)	-	219.0
Gravel Energy Storage (g)	-	28.9
Concrete Slab (c)	-	31.8

TABLE 10. INSIDE RADIATION EXCHANGE NETWORK RESISTANCES ($R \times 10^3$ ohms).

$(R_{ri})_{f_1}$	0.7168	R_{f_1c}	110	R_{pc}	360
$(R_{ri})_{f_2}$	3.74	R_{f_1g}	84	R_{pg}	387
$(R_{ri})_p$	3.49	R_{f_1d}	68	R_{pd}	498
$(R_{ri})_c$	2.9	R_{f_1h}	46.2	R_{ph}	498
$(R_{ri})_g$	2.32	R_{f_2p}	4750	R_{cd}	3580
$(R_{ri})_d$	6.8	R_{f_2c}	419	R_{ch}	120
$(R_{ri})_h$	2.18	R_{f_2g}	397	R_{gd}	3580
$R_{f_1f_2}$	95.5	R_{f_2d}	510	R_{gh}	126
R_{f_1p}	4.77	R_{f_2h}	192	R_{dh}	810

Simulation Results and Discussion

The studies described in this paper are the first phase in the application of electric circuit analogue and digital simulation analysis techniques to obtain the temperature-time response of greenhouse solar drying system for peanuts and grains. Since the rotary solar drum unit is the major heat source in the system, the surface temperatures were computed based on the daily solar radiation. Figure 32 shows the measured total solar radiation on horizontal surface, temperatures of solar drum surface, inside and outside air for November 11, 1978. High drum temperature contributed significantly in solar heating of air mass resulting in the average temperature rise of 6.6°C . The curve for predicted drum surface temperatures are in good agreement with the measured data.

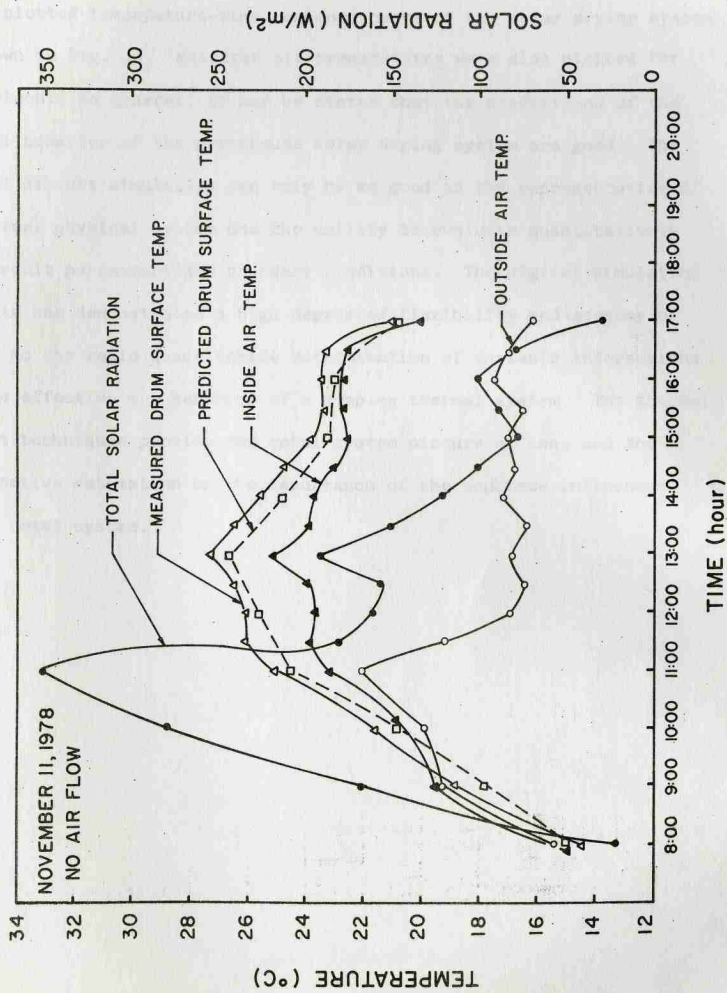


Fig. 32. Solar Radiation, Outside and Inside Air Temperatures, and Measured and Predicted Solar Drum Surface Temperatures.

The simulation analysis was performed using an electronic circuit analysis program to study the air temperature inside the solar drum. Computer plotted temperature-time response curve of the solar drying system is shown in Fig. 33. Measured air temperatures were also plotted for comparison. In general, it may be stated that the predictions of the thermal behavior of the greenhouse solar drying system are good. The thermal circuit simulation can only be as good as the representation of the actual physical system and the ability to evaluate quantitatively the circuit parameters and boundary conditions. The digital simulation analysis has demonstrated a high degree of flexibility and economy of effort in the rapid quantitative determination of variable interactions and the effect on the behavior of a complex thermal system. The thermal circuit techniques provide the total system picture at once and the quantitative estimation on the importance of the separate influences on the total system.

LATENT HEAT STORAGE SYSTEM DESIGN AND CONSTRUCTION

In previous applications gravel bed sensible heat storage system was used to store solar energy (Fig. 34). In this system solar heated air was passed through the gravel bed and heat energy was stored by raising gravel temperature. In rock or water storage units heat is stored as the rock or water increases in temperature or sensible heat storage. Another type of thermal storage system is latent heat storage through the use of phase-change materials. These materials can store large amounts of heat in the change of phase from solid to liquid (latent heat of fusion). For example, calcium chloride hexahydrate ($\text{CaCl}_2 \cdot 6\text{H}_2\text{O}$) has a latent heat of fusion of 193 kJ/kg (82 Btu/lb). The large amounts of heat that can be stored in the change of phase of these materials can reduce the storage volume 1/2 to 1/4 of that required for rock storage. Another advantage of phase-change thermal storage is that a phase-change material with a desirable phase-change temperature can be chosen for a particular solar application. In a heat storage cycle a circulating fluid (air or water) can supply heat to the storage unit causing the phase-change material to melt. In a heat dissipation cycle a circulating fluid can extract heat from the storage unit causing the phase-change material to solidify.

This chapter covers preliminary design and construction phase of a latent heat storage system to be used as an integrated part of the greenhouse solar system. Commercial cylindrical latent heat storage rods, "Thermo-81 - The Energy Rods", were used as a primary heat storage element. Two different stacking configurations were designed in order to have different air flow patterns through the system to study the heat transfer characteristics.

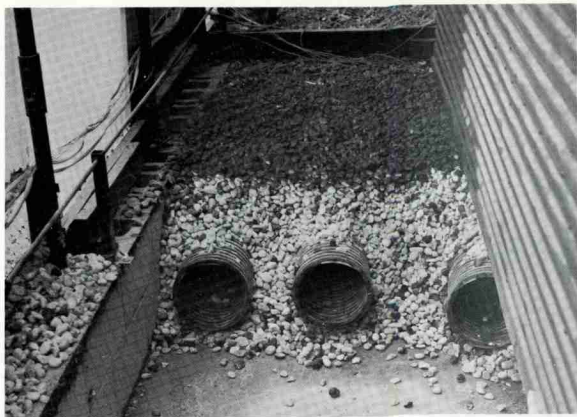


Fig. 34. Gravel Bed Sensible Heat Storage System.



Fig. 35. Experimental Clear Cylindrical Latent Heat Storage Elements.

For a typical rock bed storage, energy storage density is given $1.34 \text{ MJ}/^{\circ}\text{C}\cdot\text{m}^3$ based on a packing fraction (bulk density divided by material density) of 0.58, a density of $2650 \text{ kg}/\text{m}^3$, and a specific heat of $0.5 \text{ kJ}/\text{kg}$ [10]. By using this energy storage density one can achieve up to a $40 \text{ MJ}/\text{m}^3$ for a 30°C temperature increase. However, as shown in Table 11, energy storage density for latent heat storage is more than three times larger than this value even for the loosest stacking. Therefore, this superiority is a promising future to increase solar contribution in the greenhouse solar system.

TABLE 11. PROPERTIES OF LATENT HEAT STORAGE SYSTEM.

	UNIT 1	UNIT 2
Total number of rods	46	46
Width (m)	1.15	1.23
Length (m)	1.83	1.83
Height (m)	0.35	0.41
Volume (m^3)	0.74	0.92
Energy storage density (MJ/m^3)	161.3	129.8
Porosity	0.29	0.43
Total heat transfer area (m^2)	23.5	23.5
Passage volume (m^3)	0.22	0.40
Storage cost* ($\$/\text{m}^3$)	1865	1500

* Includes only rod cost.

Latent Heat Storage System

In this study a commercial cylindrical latent heat storage element, "Thermol 81 - The Energy Rod", was used as a primary container. The melting temperature of the phase-change material, 27°C, is almost an optimum temperature for environmental heating, grain and crops drying. The temperature is also low enough to cause the phase change by using air heated by greenhouse solar system.

In addition to the energy rods, experimental rods made of clear plastic tubes were designed and filled with similar phase-change material (PCM) to make it possible to observe phase-change process as shown in Fig. 35. The PCM used was Calcium Chloride Hexahydrate ($\text{CaCl}_2 \cdot 6\text{H}_2\text{O}$) produced by Dow Chemical Company. The thermal properties of this material are given in Table 12. The net weight of the PCM filled into these clear rods are given in Table 13.

The gravel beds on both sides of the solar barn were emptied and the bottom and side walls of the rectangular channels which were previously used for the gravel containment were insulated with 3/4" styrofoam boards. Cylindrical storage elements, the primary containers, were placed into the insulated spaces.

Two different baffle systems were used in order to obtain two air flow patterns through the rods. "Ring baffles" (Fig. 36) and cross baffles (Fig. 37) were respectively used in UNIT 1 and UNIT 2. Geometric configurations of these two systems are shown in Figs. 38 and 39 for UNIT 1 and Figs. 40 and 41 for UNIT 2. These two configurations are geometrically optimized for the channels which exist in the greenhouse solar system. Experimental study will be conducted for the two different storage systems under various climatic conditions.

TABLE 12. THERMO-PHYSICAL PROPERTIES OF CALCIUM CHLORIDE HEXAHYDRATE.

Melting temperature	27.22°C	180.996 of
The Heat of Fusion	190.72 kJ.kg ⁻¹	
Specific gravity		
Solid at 25°C	1.71 gm.cc ⁻¹	
Liquid at 40°C	1.527 "	
Specific heat		
Solid	1.423 kJ.kg ⁻¹ °C ⁻¹	
Liquid	2.218 "	
Conductivity		
Solid	1.089 W m ⁻¹ °C ⁻¹	
Liquid at 39°C	0.54 "	
Liquid at 69°C	0.561 "	

TABLE 13. NET WEIGHT OF CALCIUM CHLORIDE HEXAHYDRATE IN CLEAR RODS.

Rod No.	Net Weight (kg)
1	13.08
2	12.66
3	13.58
4	13.42
5	13.22
6	12.89

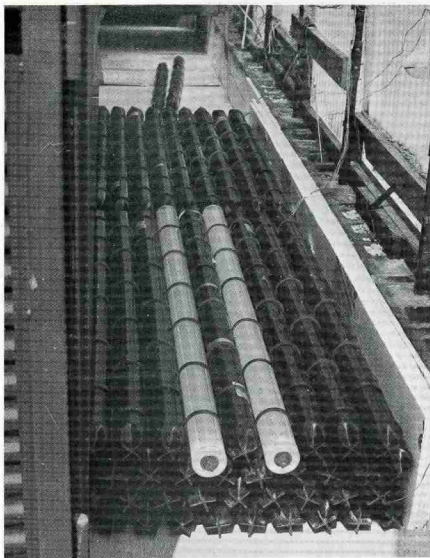


Fig. 36. Ring Baffled Storage Unit.

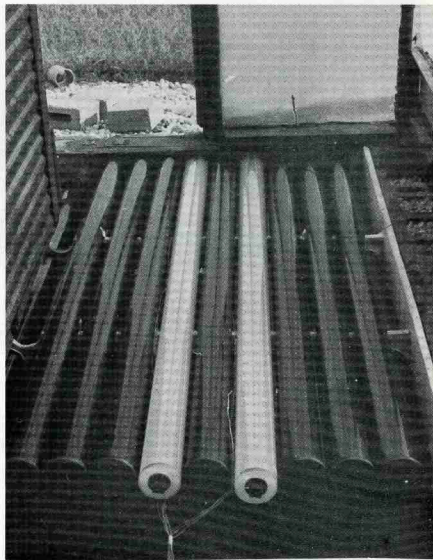


Fig. 37. Cross Baffled Storage Unit.

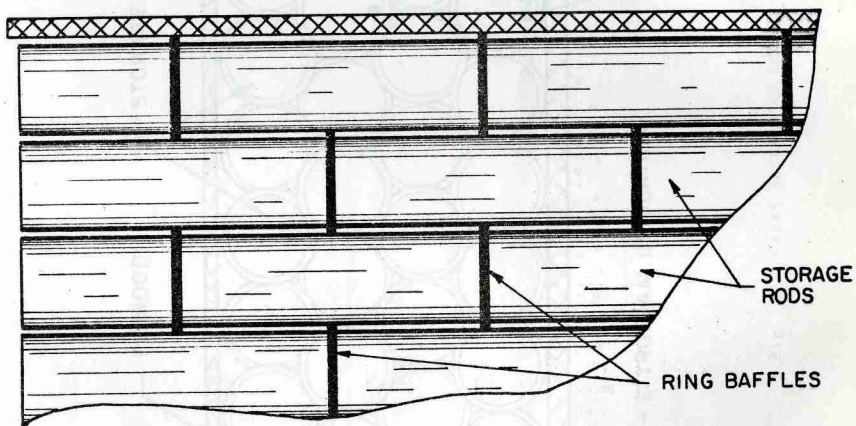
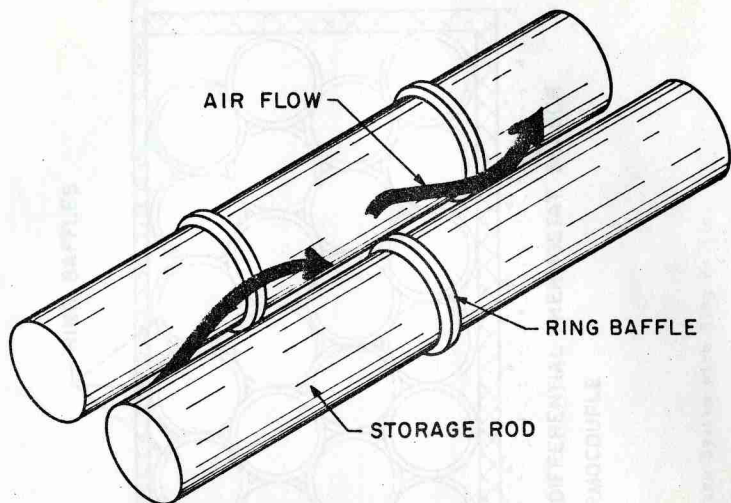


Fig. 38. Latent Heat Storage System with Ring Baffles: (a) Air Flow Pattern between Storage Rods; (b) Top View of Bottom Layer Rods and Ring Baffles Arrangement.

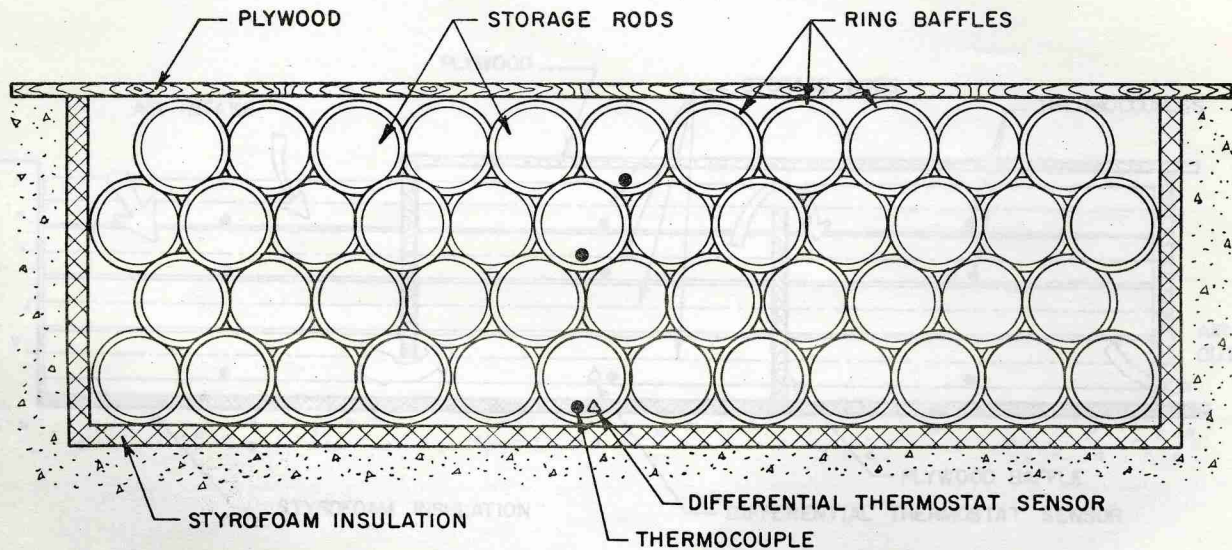


Fig. 39. Cross Section of Latent Heat Storage System with Ring Baffle.

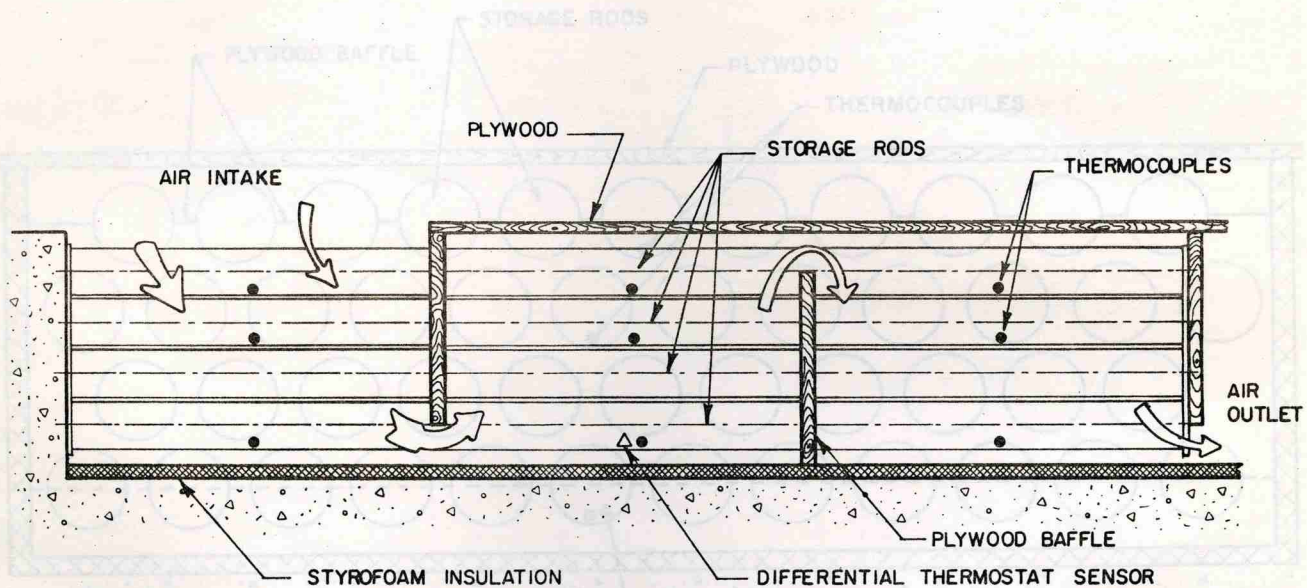


Fig. 40. Latent Heat Storage System with Cross Baffles.

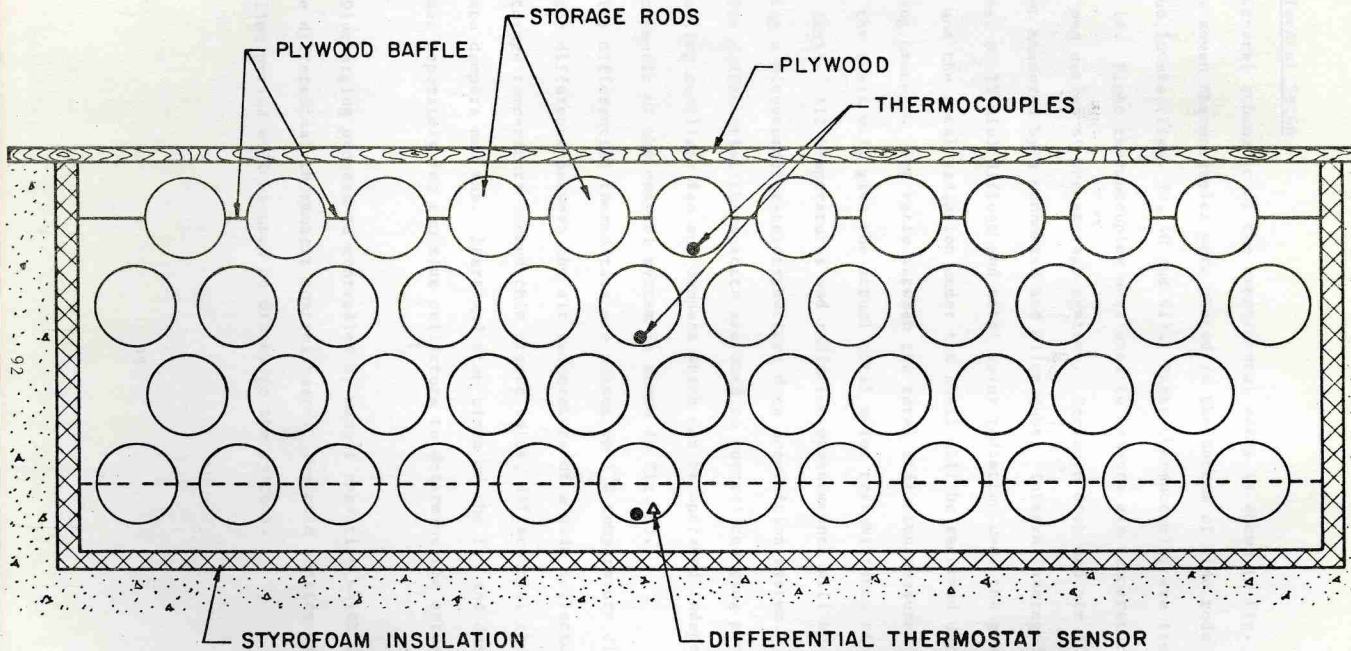


Fig. 41. Cross Section of Latent Heat Storage System with Cross Baffles.

Experimental Setup

General schematic of the experimental setup is shown in Fig. 42. Twenty seven thermocouples were placed in the bottom of nine rods at various levels (Figs. 39, 40 and 41). These thermocouples are listed in Table 14. Eight thermocouples were used to measure air temperature at the inlet and outlet of the storage systems. Pressure drop and air flow rate will be measured by a manometer and pilot tube. Integral averaged (in scan interval of 15 min) diffuse and total solar radiation over the greenhouse shell and the total radiation under the shell will be recorded during the charging process. The ratio between the total radiation measured over and under the shell will give the actual total solar transmittance of the greenhouse shell. All temperatures and radiation measurements will be recorded by using a microcomputer-teletypewriter data acquisition system.

Two differential thermostats are used to control charging process by controlling auxiliary fan and dampers which can be operated independently. The schematic of the control system is shown in Fig. 43.

The differential thermostats are preset on 5°C temperature differences. When the difference between the air temperature of a side collector and the storage temperature exceed this preset value, differential thermostats activate dampers and fan. Start and stop times of the fan and dampers are recorded separately for two side collectors to determine the actual charging time.

Discharging process is controlled by manual operation which is provided on the differential thermostat control board. The cold outside air during nighttime period will be used to discharge the systems.

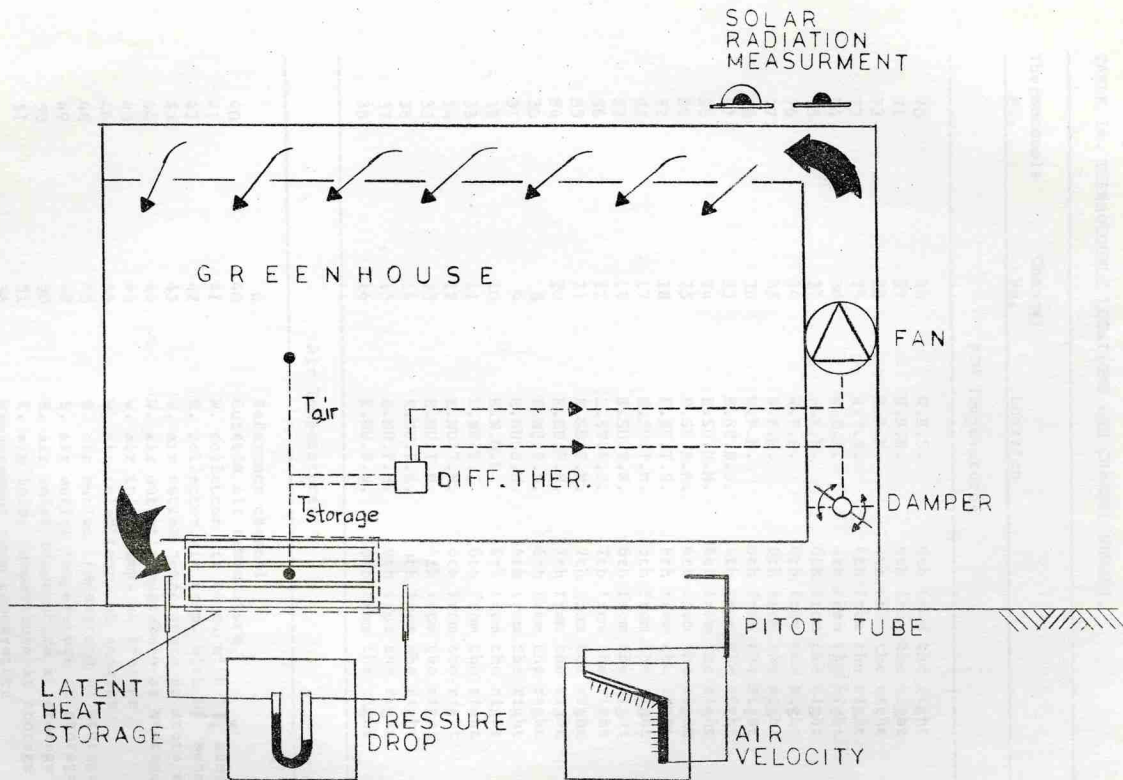


Fig. 42. Schematics of Experimental Setup.

TABLE 14. THERMOCOUPLE LOCATIONS AND CHANNEL NUMBER.

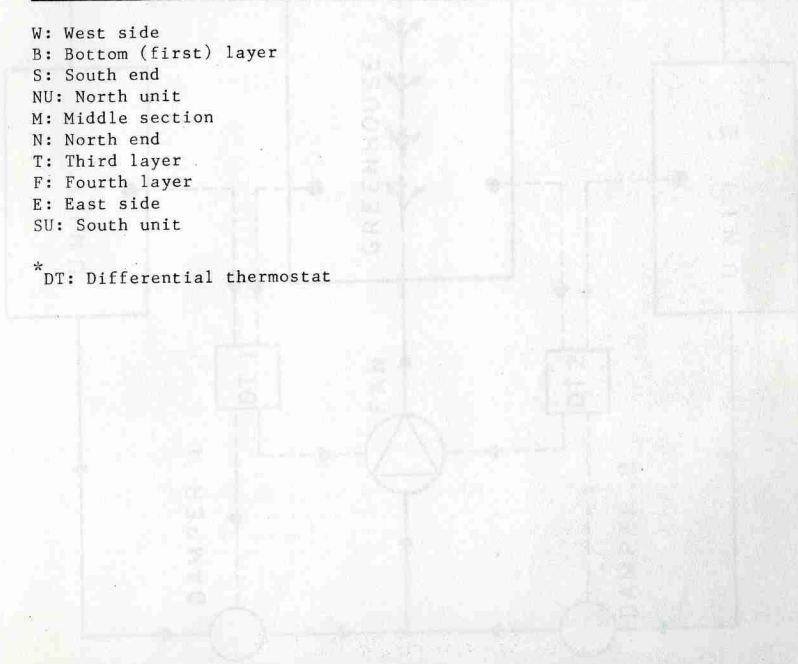
Thermocouple No.	Channel No.	Location
PCM Temperatures		
70	26	W.B.S. 6th from the right
71	27	W.B.M. 6th from the right
72	28	W.B.N. 6th from the right
73	29	W.T.S. 6th from the right
74	30	W.T.M. 6th from the right
75	31	W.T.N. 6th from the right
76	34	W.F.S. 6th from the right
77	35	W.F.M. 6th from the right
78	36	W.F.N. 6th from the right
57	23	E.SU.B.S. 6th from the right
58	24	E.SU.B.M. 6th from the right
59	25	E.SU.B.N. 6th from the right
52	18	E.SU.T.S. 6th from the right
51	17	E.SU.T.M. 6th from the right
53	19	E.SU.T.N. 6th from the right
56	22	E.SU.F.S. 7th from the right
55	21	E.SU.F.M. 7th from the right
54	20	E.SU.F.N. 7th from the right
30	8	E.NU.B.S. 6th from the right
31	9	E.NU.B.M. 6th from the right
32	10	E.N.B.N. 6th from the right
33	11	E.NU.T.S. 6th from the right
34	12	E.NU.T.N. 6th from the right
35	13	E.NU.T.N. 6th from the right
36	14	E.NU.F.S. 6th from the right
37	15	E.NU.F.M. 6th from the right
38	16	E.NU.F.N. 6th from the right
Air Temperatures		
	6	Reference channel
40	40	Outside air temperature
41	41	W. collector air temp. with DT_x^* sensor
42	42	E. collector air temp. with DT_x sensor
43	43	W. air outlet temperature at storage
44	44	W. air outlet temperature at storage
45	45	W. air inlet temp. at storage
46	46	W. air inlet temp. at storage
48	48	E. air outlet temperature at storage
49	49	E. air outlet temperature at storage
50	50	E. air inlet temperature at storage
51	51	E. air inlet temperature at storage
-	56	Measurement room temperature

TABLE 14. CONT'D:

Thermocouple No.	Channel No.	Location
Solar Radiation		
	1	Total radiation over greenhouse shell
	2	Diffuse radiation over greenhouse shell
	3	Total radiation under greenhouse shell

W: West side
 B: Bottom (first) layer
 S: South end
 NU: North unit
 M: Middle section
 N: North end
 T: Third layer
 F: Fourth layer
 E: East side
 SU: South unit

* DT: Differential thermostat



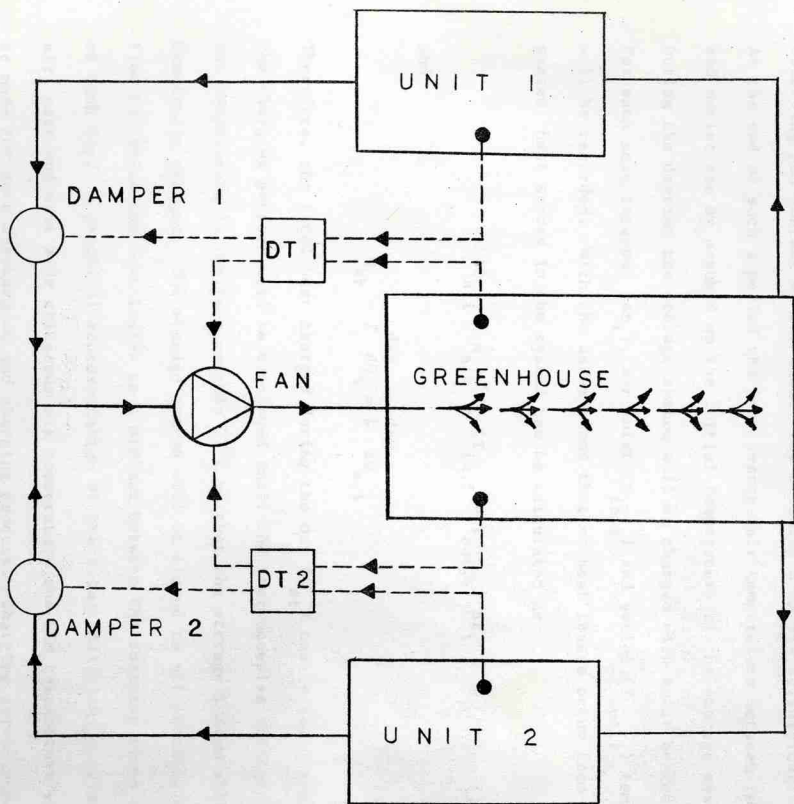


Fig. 43. Schematic of Control System.

Methods and Procedures

The cold outside air will be passed through the systems until the all PCM in the rods are solid. These assumptions can be made valid by observing PCM content of the clear rods becoming complete solidification. At the end of such a period the last average air temperature between inlet and outlet can be assumed as the initial temperature of the storage system. During the daytime the storage system will be charged with solar heated air. For each scan interval (Δt_i), air inlet ($T_{in,i}$) and outlet ($T_{out,i}$) temperature will be recorded. With the assumptions that no heat losses occur from the system, heat stored in the system can be calculated as

$$\Delta Q_{s,i} = \dot{m}_{air} C_p (T_{in,i} - T_{out,i}) \Delta t_i \quad (75)$$

and

$$Q_{st} = \int_{day} dQ_s \approx \sum_{day} \Delta Q_{s,i} \quad (76)$$

Therefore, the total heat charged during the day (Q_{st}) can be calculated. The charging process will be continued until the thermocouples indicate that the temperature in the rods exceeds 27°C so that the storage system will be completely charged. The storage system will be closed to all possible air flow to reduce the heat losses to a minimum between the charging steps held on each day. A graphical representation of the solar radiation, outside air, east and west side collector air temperature and PCM temperature will be made for each discharging and charging process. Charging curve (cumulated $\Delta Q_{s,i}$ versus time) will be presented on the graph to evaluate the characteristics of latent heat storage system.

REFERENCES

1. ASHRAE. 1977. Handbook of Fundamentals.
2. Bowers, C.G., Jr., B.K. Huang and A.H. Nassar. 1978. Solar energy drying and process control with microcomputer. ASAE Paper No. 78-3537.
3. Bowers, C.G., Jr., B.K. Huang and D.H. Willits. 1976. Improving solar energy collection, storage, and air flow control in greenhouse solar curing barn. ASAE Paper No. 76-3548.
4. Bowers, C.G., Jr., B.K. Huang and C.F. Abrams, Jr. 1975. Solar energy utilization in a bulk curing/greenhouse system. ASAE Paper No. 75-3504.
5. Brooker, D.B., B.A. McKenzie and H.K. Johnson. 1978. The present status of on-farm grain drying. ASAE Paper No. 78-3007.
6. Butler, J.L. and J.M. Troeger. 1977. Use of solar energy to cure peanuts. ASAE Paper No. 77-3033.
7. Calderwood, D.L. 1977. Rice drying with solar heat. ASAE Paper No. 77-3003.
8. Chang, H.S. 1977. Solar energy utilization in a bulk curing and drying system. Journal of Chinese Agricultural Engineering, 23(2).
9. Chen, C.S. and W.H. Johnson. 1969. Kinetics of moisture movement in hygroscopic materials II (an application to foliar materials). Trans. of ASAE 12(4):478-481.
10. Connor, W. 1980. Low temperature sensible heat storage. Solar Energy Technology Handbook, Part A.
11. Converse, H.H., G.H. Foster and D.B. Sauer. 1977. Low temperature grain drying with solar heat. ASAE Paper No. 76-3018.
12. Cundiff, J.S. 1981. A renewable resources system for curing tobacco. Agric. Energy, ASAE Pub. 3-81, 1:59-65.
13. Duffie, J.A. and W.A. Beckman. 1974. Solar Energy Thermal Process. John Wiley and Sons.
14. Foster, G.H. and R.M. Peart. 1976. Solar grain drying progress and potential. Agric. Inf. Bul. No. 401.
15. Green, T.F. and G.C. Vliet. 1979. Transient response of a latent heat storage unit: an analytical and experimental investigation. ASME Paper No. 79-HT-36.
16. Hill, J.E. and T. Kusuda. 1974. Method of testing for rating solar collectors based on thermal performance. National Bureau of Standards. Report No. NBSIR-74-639.

17. Hottel, H.C. and B.B. Woertz. 1942. The performance of flat-plate solar heat collectors. ASME Trans. 64:91-104.
18. Huang, B.K., M.N. Ozisik and M. Toksoy. 1981. Development of greenhouse solar drying for farm crops and processed products. AMA 12(1):47-52.
19. Huang, B.K. and M. Toksoy. 1981. Greenhouse solar system for effective year-round solar energy utilization in agricultural production. Agric. Energy, ASAE Pub. 3-81, 1:152.
20. Huang, B.K. and M. Toksoy. 1981. Thermal analysis of a greenhouse solar bulk curing and drying system. ASAE Paper No. 81-4042.
21. Huang, B.K. and C.G. Bowers, Jr. 1980. Automated container-grown seedling production for automatic transplanting. Proc. SNA Research Conf., p. 199-203.
22. Huang, B.K. 1980. Effective solar energy utilization in tobacco production with greenhouse bulk curing solar barn. Inf. Bul. 7th International Tobacco Scientific Congress, Manila, Philippines, p. 61.
23. Huang, B.K. 1979. Energy in agriculture. Proc. First International Symposium on Policy Analysis and Information Systems, Durham, N.C., p. 36-46.
24. Huang, B.K. and N.M. El-Shaik. 1979. Simulation analysis of greenhouse solar drying system for peanuts and grains. ASAE Paper No. 79-3082.
25. Huang, B.K., C.G. Bowers, Jr. and A.H. Nassar. 1979. Greenhouse solar system for bulk curing tobacco and peanuts. Proc. Use of Solar Energy for Crop Drying Conf., Atlanta, GA.
26. Huang, B.K. and C.G. Bowers, Jr. 1977. Solar-energy utilization using greenhouse bulk curing and drying system. Proc. Solar Crop Drying Conf., Raleigh, N.C., p. 117-145.
27. Huang, B.K. and A.H. Nassar. 1977. Hydroponic plant production in greenhouse bulk curing solar barn. ASAE Paper No. 77-1012.
28. Huang, B.K. and H.S. Chang. 1976. Circuit simulation analysis of heat transfer effect in solar drying. ASAE Paper No. 76-3019.
29. Huang, B.K. and C.G. Bowers, Jr. 1976. Immediate solar-energy utilization using greenhouse bulk curing and drying system. Final Report PTP74-17622. 71 pp.
30. Huang, B.K., C.F. Abrams, Jr., L.L. Coats and C.G. Bowers, Jr. 1975. Development of greenhouse bulk drying systems for solar energy utilization and plantbed mechanization. ASAE Paper No. 75-1018.
31. Huang, B.K. 1973. Systems engineering of precision automatic transplanting. ASAE Paper No. 73-104.

32. Husain, A., C.S. Chen and J.T. Clayton. 1973. Simultaneous heat and mass diffusion in biological materials. Jour. Agric. Eng. Res., 18:343-354.
33. Johnson, W.H. 1979. Solar energy and heat recycling in tobacco curing. ASAE Paper No. 79-3568.
34. Kelly, G.E. and T.E. Hill. 1975. Method of testing for rating thermal storage devices based on thermal performance. National Bureau of Standards. Report No. NBSIR-74-634.
35. Khe, C. 1971. Analysis of a matrix solar collector for low temperature applications. Ph.D. Dissertation. University of California, Davis.
36. Kline, G.L. 1977. Solar collectors for low temperature grain drying. ASAE Paper No. 77-3007.
37. Liu, B.Y.H. and R.C. Jordan. 1963. A rational procedure for predicting the long-term average performance of flat-plate-solar energy collectors. Solar Energy, 7(2):53-70.
38. McLendon, B.D. and J.M. Allison. 1978. Solar energy utilization in alternate grain drying systems in the Southeast. ASAE Paper No. 78-3013.
39. Milburn, W.F., R.A. Aldrich and J.W. White. 1977. Internal/external solar collectors for greenhouse heating. ASAE Paper No. 77-4008.
40. Morey, R.V., H.A. Cloud, R.J. Gustafson and D.W. Peterson. 1977. Evaluation of the feasibility of solar energy grain drying. ASAE Paper No. 77-3013.
41. Nassar, A.H., B.K. Huang and C.G. Bowers, Jr. 1979. Microcomputer control in greenhouse bulk curing and drying solar systems. ASAE Paper No. 79-3083.
42. Nassar, A.H., B.K. Huang and P. Oppenheim. 1979. Greenhouse solar system control with microcomputer. ASAE Paper No. 79-4030.
43. Nassar, A.H., B.K. Huang and C.G. Bowers, Jr. 1978. A microcomputer-based control system for solar energy utilization in greenhouses. Proc. SNA Research Conf., p. 123-127.
44. Oppenheim, P. and B.K. Huang. 1980. The operation and control of a solar system adapted to conventional bulk curing barns. ASAE Paper No. 80-3070.
45. Ozisik, M.N., B.K. Huang and M. Toksoy. 1980. Solar grain drying. Solar Energy, 24(4):397-401.
46. Sarmiento, I.A., B.K. Huang and C.F. Abrams, Jr. 1980. Automatic transplanting of individual tobacco seedlings. Inf. Bul. 7th International Tobacco Scientific Congress, Manila, Philippines, p. 75-76.
47. Tabili, R.G. and R.T. Pagtulingan. 1978. Summary data on three curing tests on Taiwan solar barn. Philippine Virginia Tobacco Administration.

48. Threlkeld, J.L. 1962. Thermal Environmental Engineering. Prentice-Hall, Inc., Englewood Cliffs, Chap. 14, p. 309-334.
49. Walton, L.R., W.H. Henson, Jr., S.G. McNeil, B.F. Parker and J.M. Bunn. 1977. Solar curing facilities for burley tobacco. ASAE Paper No. 77-3002.
50. Willits, D.H., C.G. Bowers, Jr., P.V. Nelson and B.K. Huang. 1976. A solar energy storage system for greenhouse. ASAE Paper No. 76-3507.
51. Young, J.H. and T.B. Whitaker. 1971. Evaluation of the diffusion equation for describing thin-layer drying of peanuts in the hull. Trans. ASAE 14(2):309-312.